machines

MDPI

Article

Hybridization of a Backhoe Loader: Electric Drive System Design

Dener A. de L. Brandao [1,*], Mariana de F. Ramos [1], Thiago M. Parreiras [1,2], Thales A. C. Maia [3], Igor A. Pires [4], Tomás P. Corrêa [4], Braz de J. Cardoso Filho [3] and Anderson Nascimento [5]

1 Graduate Program in Electrical Engineering, Universidade Federal de Minas Gerais, Belo Horizonte 31270-901, Brazil
2 Institute of Technological Sciences, Universidade Federal de Itajubá, Itabira 35903-087, Brazil
3 Department of Electrical Engineering, Universidade Federal de Minas Gerais, Belo Horizonte 31270-901, Brazil
4 Department of Electronic Engineering, Universidade Federal de Minas Geraiss, Belo Horizonte 31270-901, Brazil
5 South America Tractor Backhoe Loader, CNH Industrial Brasil, Contagem 32210-900, Brazil
* Correspondence: dener.brandao@ieee.org

Abstract: Heavy machinery is critical to agriculture, construction, mining, and other sectors of a country's economy. However, such vehicles consume a high amount of fuel, increasing production costs and the emission of polluting gases into the atmosphere. One of the alternatives to reduce fuel consumption is the electrification of these vehicles, but the definition of an optimal topology for the electrification of heavy vehicles is still under study, and works with electric drive systems projects for these machines are scarce. This paper presents the main characteristics of the design of an electric drive system for the electrification of a backhoe, including the control and simulation of the motor drive system, and presents a prototype bench and experimental tests carried out in the context of the hybridization topology presented. Based in these results, improvements are proposed and discussed with aid of computational simulation.

Keywords: heavy construction machinery; hybrid vehicle; drive system; backhoe loader; off-road vehicle

Citation: Brandao, D.A.d.L.; Ramos, M.d.F.; Parreiras, T.M.; Maia, T.A.C.; Pires, I.A.; Corrêa, T.P.; Cardoso Filho, B.d.J.; Nascimento, A. Hybridization of a Backhoe Loader: Electric Drive System Design. *Machines* **2023**, *11*, 471. https://doi.org/10.3390/machines11040471

Academic Editor: Dan Zhang

Received: 28 February 2023
Revised: 26 March 2023
Accepted: 5 April 2023
Published: 12 April 2023

1. Introduction

The use of vehicles for locomotion and services is one of the fundamental sectors of a country's economy. According to a document from the US Department of Energy, there are about 253 million light vehicles and about 13.5 million heavy trucks in the United States. Heavy trucks and buses accounted for 11% of the 2.9 trillion vehicle miles driven in 2020 [1]. Despite representing 11% of the total miles traveled, heavy trucks and buses consumed about 19% of all oil used in the country, which consumes 19.8 million barrels of petroleum per day.

With a high expenditure on fossil fuels, vehicle electrification comes as an alternative to reduce the consumption of heavy vehicles and, consequently, reduce the emission of polluting gases into the atmosphere [2]. With these objectives in mind, some hybrid construction machinery (HCM) manufacturers have hybridized the traction system or the hydraulic implements of their vehicles responsible for the higher consumption of equipment such as bulldozers [3]. The Volvo L220F Hybrid, Mecalac 12MTX Hybrid, and John Deere 664K Hybrid models carry out parallel hybridization of the wheel loader or articulated loader. Kobelco SK200H Hybrid and Komasu HB215 LC-1 models perform hybridization of the excavator, in series and parallel topologies, respectively, and use supercapacitors for energy storage [4].

Several of these models share a commonality in that they are a hybrid version of an existing conventional model. In this way, there is a reduction in expenses, as it is not

necessary to make significant changes in the production process of existing machines. However, this choice brings limitations to the electric drive system design.

The literature on electrification of heavy vehicles is scarce [5] and does not cover all aspects of electric drive system design in depth. Some of these works are presented in [6,7], but they focus on the mechanical aspects to encompass the hybrid solution. Another work addresses the hybridization of military vehicles, but focusing only on the design of the electric motor and the energy storage system [8]. The authors in [9] analyze the feasibility of electrifying agricultural machinery, with emphasis on the design of the electric motor and the cooling system. Something similar is described in [10], but the design aspects of the electric drive system are not addressed. The electric motor performance requirements and design are carried out in [11], without addressing other components of the electrical system. The electrification of a hydraulic excavator with a speed and displacement variable pump is presented in [12], achieving a reduction in idle consumption from 2.05 kW to 0.7 kW, but without emphasis on the electrical system design. Other works address the electrification of heavy-duty off-road vehicles but focus on energy management aspects [13–16].

The main contribution of this paper is to present a complete and adequate electric drive system in the context of the series hybridization of a backhoe loader with batteries, taking into account the technical aspects of the normative aspects related to vehicle electrification. The specification of all necessary items is presented, along with of a model bench for testing prior implementation in a backhoe loader prototype. As the correct implementation and adjustment of the motor drive control plays a crucial rule in the proper performance of any electrical vehicle, this topic is also discussed focused in the implemented system. Experimental results are obtained in a laboratory. An analysis of the drive system control focused on the backhoe hybridization, its operating profile and the control improvements that can be implemented are discussed and simulated.

2. Technical Standards

For the design of the electric drive system to be safe and functional, it must meet the technical standards relevant to the subject of vehicle electrification. The main institutions dealing with technical standards related to vehicle electrification are the International Organization for Standardization (ISO), the International Electrotechnical Commission (IEC), the Institute of Electrical and Electronics Engineers (IEEE), and SAE International. Table 1 shows some of the main international standards related to light and heavy vehicles electrification.

Table 1. Some technical standards related to vehicle electrification.

Standard	Title	Last Version
Regulation No. 100 [17]	Uniform provisions concerning the approval of vehicles with regard to specific requirements for the electric power train	2022
ISO 6469-2:2022 [18]	Electrically propelled road vehicles—Safety specifications—Part 2: Vehicle operational safety	2022
ISO 6469-3:2021 [19]	Electrically propelled road vehicles—Safety specifications—Part 3: Electrical safety	2021
ISO 6722-1:2011 [20]	Road vehicles—60 V and 600 V single-core cables—Part 1: Dimensions, test methods and requirements for copper conductor cables	2011

Table 1. *Cont.*

Standard	Title	
ISO 17409:2020 [21]	Electrically propelled road vehicles—Conductive power transfer—Safety requirements	2020
ISO 15118-1:2019-1 [22]	Road vehicles—Vehicle to grid communication interface—Part 1: General information and use-case definition	2019
ISO 26262-1:2018 [23]	Road vehicles—Functional safety—Part 1: Vocabulary	2018
BS EN 60529:1992+A2:2013 [24]	Degrees of protection provided by enclosures (IP Code)	2013
BS EN IEC 61851-1:2019 [25]	Electric vehicle conductive charging system—General requirements	2019
IEC 62485-3:2014 [26]	Safety requirements for secondary batteries and battery installations—Part 3: Traction batteries	2013
SAE J2344 [27]	Guidelines for Electric Vehicle Safety	2020
SAE J1797 [28]	Recommended Practice for Packaging of Electric Vehicle Battery Modules(STABILIZED Aug 2016)	2016
SAE J1939 [29]	Serial Control and Communications Heavy Duty Vehicle Network—Top Level Document	2018

3. Hybridization Strategies

The electrification of heavy machinery can be achieved both in the traction system and the system of the vehicle's hydraulic implements. Regardless of which system is electrified, electrical drive, cooling, communication, and energy management systems must be designed. In this work, the focus will be on the design of the electric drive system, as shown in Figure 1.

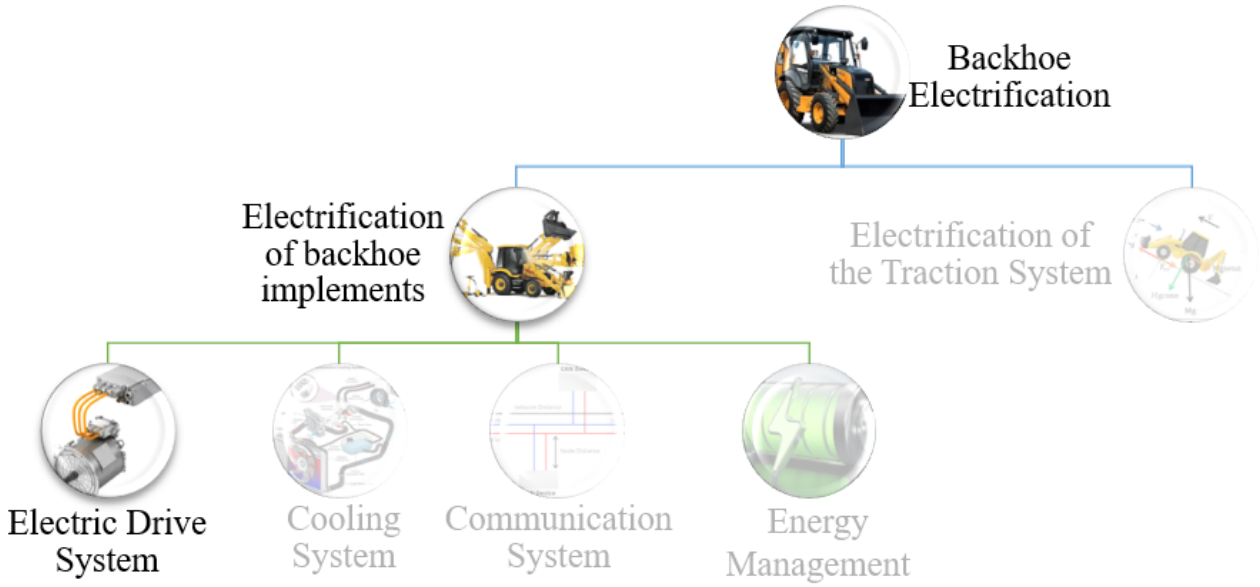

Figure 1. Scheme of the electrification project of a heavy machinery.

Once the vehicle system to be electrified is defined, the first step to size the electrification components that make up the backhoe electrical system is to define the topology. One of the options that provide an increase in efficiency is the direct electrification of working hydraulics [30]. However, a drive controller and an electric machine are required to replace each hydraulic actuator, increasing construction costs and design complexity.

Purely electrical systems lead to disadvantages such as the high number of batteries allocated in the vehicle chassis, the need for a fast charging infrastructure, and the removal

of vehicles from operation for a few hours to recharge [31]. Thus, hybrid topologies are more suitable to achieve at this point.

3.1. Parallel Configuration

In the parallel configuration, shown in Figure 2, the mechanical power output of the internal combustion engine (ICE) is connected to the mechanical power input/output of the electric machine through a power divider [32]. The excess power of the combustion engine can be converted to electrical energy and, when necessary, the electric motor can work together with the ICE to supply power to the vehicle.

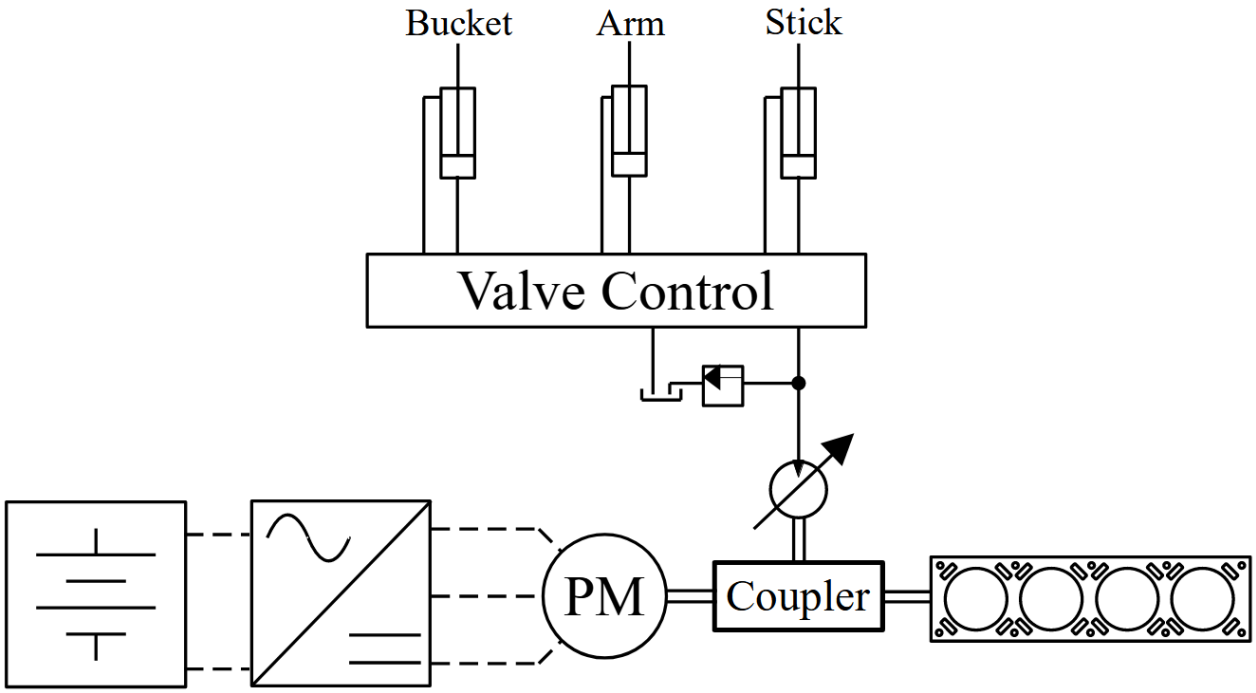

Figure 2. Parallel configuration applied to the implements of a backhoe.

It is a cheaper configuration than the others, since a single electrical machine is used as a motor and generator. With the use of a disconnect clutch, the topology allows purely mechanical or purely electrical operation in case of problems or technical needs. Its main drawback is power management, as it has fewer degrees of freedom.

3.2. Series Configuration

In the series configuration shown in Figure 3, the mechanical power of the ICE is converted into electrical power through a generator coupled with the engine shaft. The power is used to charge the storage systems and, depending on the energy management strategy, feed the electric motor that will act on the traction or the actuators of the vehicle's hydraulic implements.

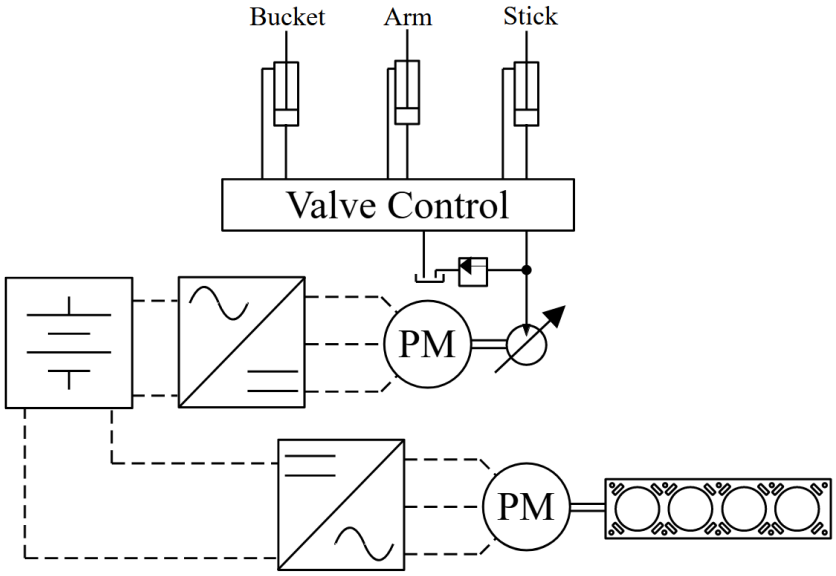

Figure 3. Series configuration applied to the implements of a backhoe.

This topology has a higher cost, since it generally requires an electrical machine, an inverter, and a dc/dc converter more than the parallel topology, and an eventual failure in the electrical drive completely prevents the operation of the machinery. However, this topology allows a greater degree of freedom in energy management, allowing us to operate the ICE in a region of better efficiency [33].

3.3. Series-Parallel Configuration

In the series-parallel configuration, shown in Figure 4, the ICE is connected to both a generator and a power divider coupled with an electric motor [4]. It has the advantages of both configurations, but with a higher price, in addition to greater control complexity.

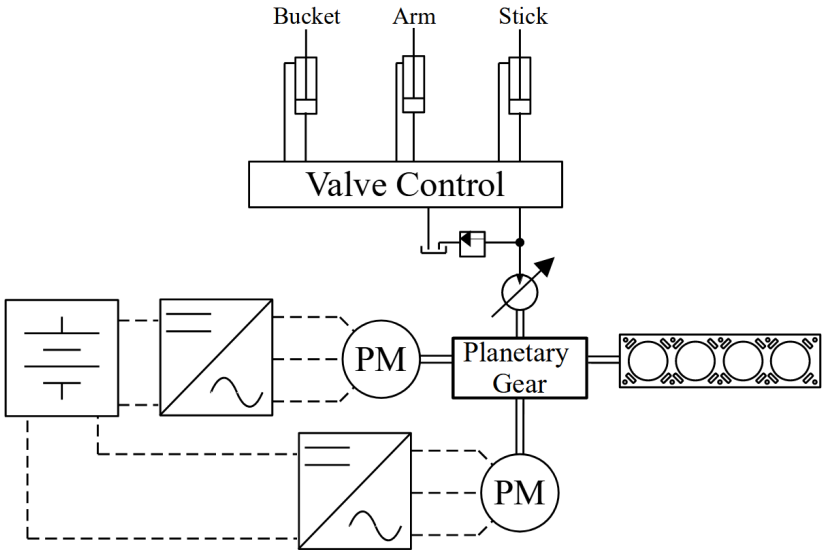

Figure 4. Series-parallel configuration applied to the implements of a backhoe.

4. Working Power

As the operation of the backhoe loader implements is the main responsible for the consumption of this type of machinery, both by the order of magnitude of the power demanded and by the operating time in a cycle of the machine [3], the hybridization of the backhoe loader present in this work focuses on aiding the operation of this movement. The

internal combustion engine used in the backhoe in this work operates in regions of low energy efficiency. Under these conditions, if there is no replacement of the ICE for another that operates in regions of better efficiency, the series topology is the most appropriate, since the degrees of freedom provided can lead the internal combustion engine to operate more efficiently [34,35], which can compensate for losses from multiple energy conversions.

In backhoe loaders, the variable load causes the ICE to work in points of low energy efficiency. The energy management strategy adopted was based on the work of [36], in which rule-based energy management is applied. When the battery state-of-charge (SoC) drops below a predefined threshold, the ICE and generator will turn on. The generator will demand from the ICE power that makes it work in regions of better efficiency, but the SoC variation of the battery is always positive. When the battery achieves full charge, the ICE and generator will shut down and the backhoe implements will operate in electric mode only. The Figure 5 below shows a flowchart of the adopted strategy.

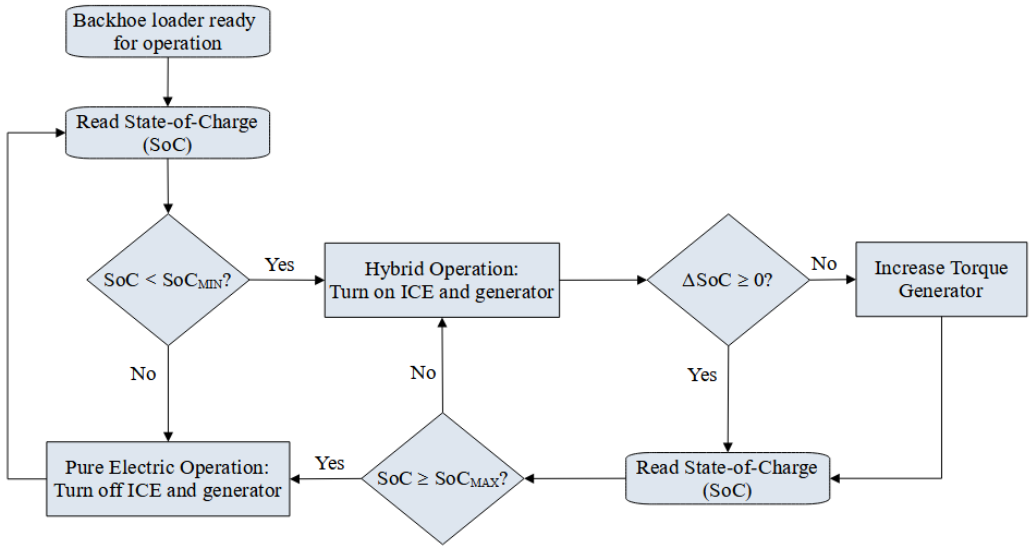

Figure 5. Energy management strategy flowchart.

Although the energy management strategy is not the focus of the work, the load characteristic of the implements is one of the inputs for energy management and is fundamental to the design of the electric drive system. Figure 6 shows the power demand of the backhoe hydraulic pump during just over 5 min of operation of the backhoe for the ditch excavation operation. Such data were obtained through field measurements of a real machine in operation.

The trenching cycle is typically performed at 20 s intervals. For each interval, the maximum and average power were evaluated, as shown in Table 2, highlighting the highest average power obtained in cycle 2 and the highest maximum power obtained in cycle 6, presented in Figure 7. As noted, the electric motor must be capable of delivering a maximum average power of 20.9 kW and a maximum power of 35.3 kW to the backhoe hydraulic pump. Operating at a speed of 1800 rpm, the maximum average torque is 110.9 Nm and the maximum peak torque is 187.3 Nm.

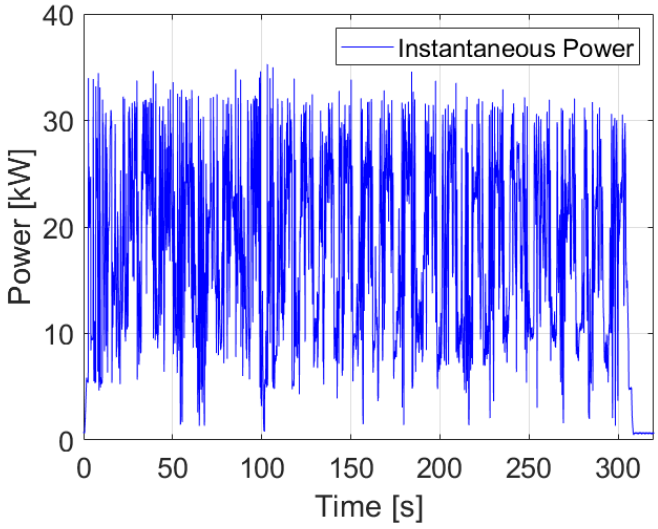

Figure 6. Power demand of the backhoe hydraulic pump in ditch excavation operation.

Table 2. Powers during backhoe operating intervals during ditch excavation.

Cycle	P_{max} (kW)	P_{avg} (kW)	Cycle	P_{max} (kW)	P_{avg} (kW)
1	34.4	15.3	9	32.8	17.2
2	34.6	20.9	10	34.6	18.6
3	33.6	19.0	11	33.5	17.1
4	32.9	16.6	12	32.9	17.8
5	34.8	19.6	13	32.2	19.6
6	35.3	15.7	14	32.0	16.9
7	32.5	20.1	15	31.7	16.0
8	33.8	17.8	16	30.5	6.9

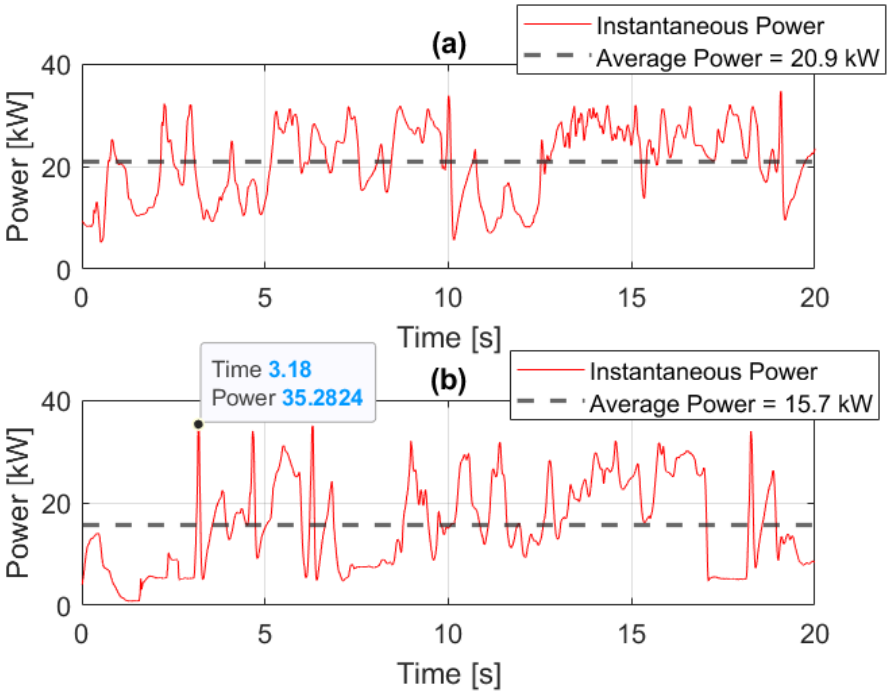

Figure 7. (**a**) Operating power during cycle 2. (**b**) Operating power during cycle 6.

5. Power Components Design

5.1. Batteries and Battery Management System

The energy storage element is fundamental in the context of the hybridization of heavy vehicles. Among the electrical energy stores, batteries have the highest energy density among the possibilities, while supercapacitors have a high power density. In any case, medium and small machines generally use only batteries [37].

For the design of the battery bank, one must take into account the power, energy, and volume available for the allocation of batteries in the vehicle, in addition to the acquisition cost. In this sense, lithium-ion batteries have the highest energy density. As the backhoe's hybridization project does not aim to change the chassis of the current model, the space available for the entire hybridization apparatus is reduced and priority will be given to reducing the volume of the batteries.

Considering the volume available for the allocation of batteries in the front part of the vehicle (about 70 L), the battery bank was dimensioned with this boundary condition. In this sense, the battery bank will be composed of four modules from the pack of Tesla Model S batteries, whose main parameters can be seen in Table 3.

Table 3. Backhoe battery bank parameters.

Modules in series	4
Capacity	5.2 kWh
Energy density	198 Wh/kg
Minimum voltage	72 V
Maximum voltage	100.8 V
Nominal voltage	88.8 V
Nominal current	233 A
Maximum discharge power (3 s)	120 kW
Continuous discharge power	20 kW
Maximum power charge (10 min)	32 kW
Continuous charge power	20 kW
Discharge current (10 s)	1000 A
Weight	105.2 kg
Dimensions	0.68 × 0.30 × 0.32 m
Volume	65.3 l

The battery bank meets the maximum volume requirements in addition to having the power capacity to handle both the maximum power and the minimum power of the electric motor coupled to the hydraulic implements.

In addition to the battery bank, it is necessary to specify the battery management system (BMS). The BMS aims to manage the energy of the battery bank to keep it within a safe operation region, performing the balancing, temperature monitoring, and charge and discharge currents of the cells during operation. The most important factors to be evaluated in the BMS specification are:

- Number of cells compatible with the battery bank;
- Protection functions: connection to the power relay and, for plug-in vehicles, control of battery charger activation.

5.2. Electric Machines and Inverters

Permanent magnet electric machines are currently the most used in electric and hybrid vehicles due to their high efficiency and high torque density [38,39]. Furthermore, permanent magnet machines with axial flux have an even higher torque density [40,41].

The battery bank of commercial electric vehicles normally has a nominal voltage of around 400 V, and some models work with voltages of up to 800 V [42,43]. As a result, there are not many high-power, low-voltage commercial machines, and inverters.

In addition to the operating voltage, the choice of electric machines must take into account the power and torque at the operating speed of the hydraulic pump of the implements. To operate the implements of a backhoe, the ICE operates at a fixed speed, around 2000 rpm, depending on the machine [3].

To meet the established voltage and power levels, the EMRAX 228 LV [44] electric machine, seen in Figure 8, was defined to compose the backhoe hybridization system, as it has a nominal power of 52 kW with a mass of 12.4 kg, giving a total power density of 4.2 kW/kg. For volume reduction, the cooling of electrical machines used in vehicular applications is liquid. Another feature of the machine is the external rotor, as shown in Figure 8.

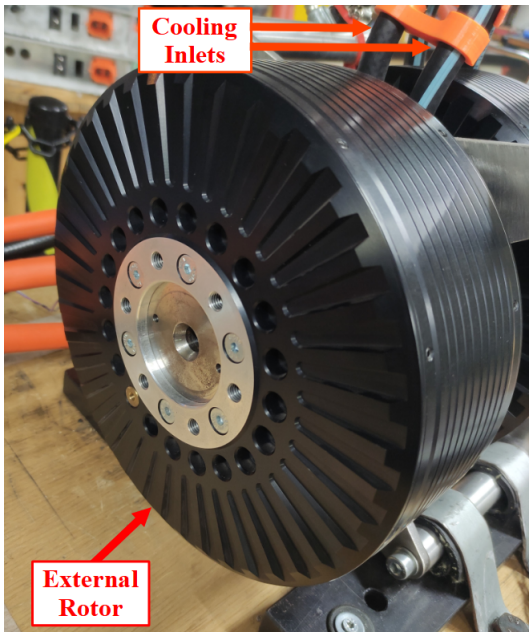

Figure 8. EMRAX 228 Low Voltage Liquid Cooled.

One of the characteristics of the motor shown in Figure 8, which allows for volume reduction, is the use of liquid cooling, which is also used in inverters for vehicular applications for volume reduction and a consequent increase in power density [45].

Although the nominal values of the machine meet the design standards, it is necessary to verify the power and torque delivered by the machine at the operating speed of the hydraulic pump. Figures 9 and 10 show the power and torque curves of the EMRAX 228 Low Voltage Liquid Cooled (LV LC) motor, highlighting the values at 1800 rpm, the speed used to operate the hydraulic pump. The power and torque values are greater than the necessary values obtained in the Section 4 and, therefore, meet the requirements for operation.

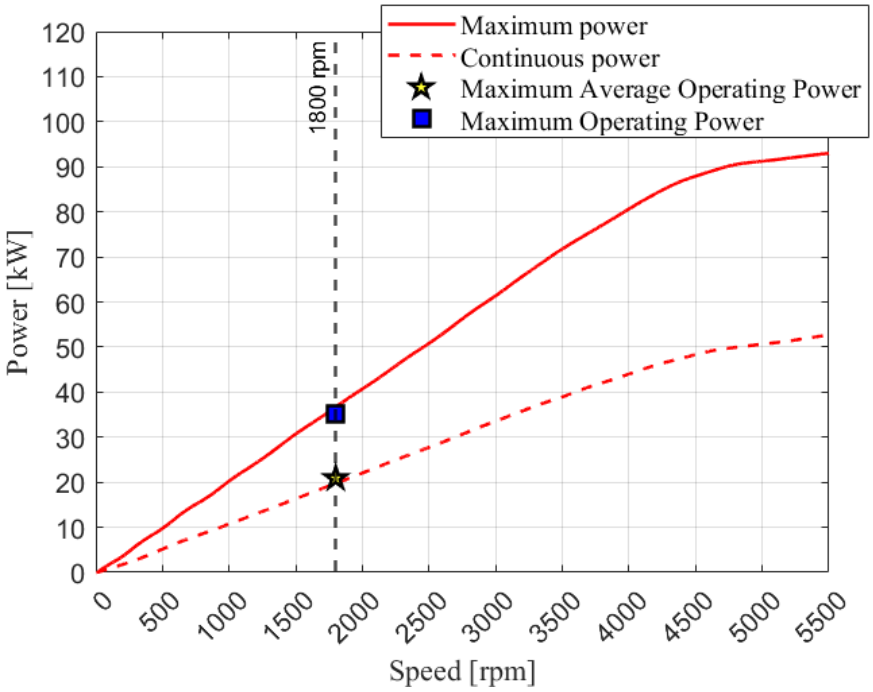

Figure 9. EMRAX 228 LV LC power curves.

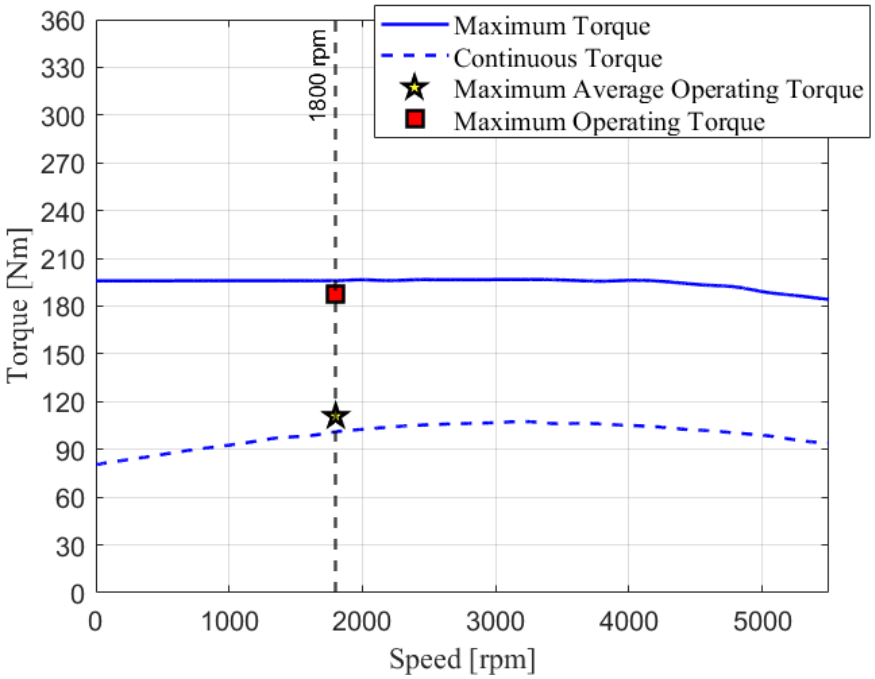

Figure 10. EMRAX 228 LV LC torque curves.

As with electrical machines, there are not many commercial inverter solutions with a high power and low voltage dc link. For the specification of the inverter, the voltage, power, and current levels compatible with the use of electrical machines, both continuously and in overload states, must be taken into account. Attention should also be paid to the communication protocol used so that there is compatibility with the other elements of the system. SAE J1939 is the standard for implementing the communication protocols in heavy-duty vehicles [29].

One of the solutions that meet the requirements of the electric machine is the inverter EmDrive 500 [46], shown in Figure 11, which meets the defined voltage levels and power levels necessary for full operation in the backhoe. As shown in Figure 11, inverters used in vehicular applications are reduced in size due to liquid cooling. One of the communication protocols available on this inverter is CANOpen [47], based on the Controller Area Network (CAN) protocol.

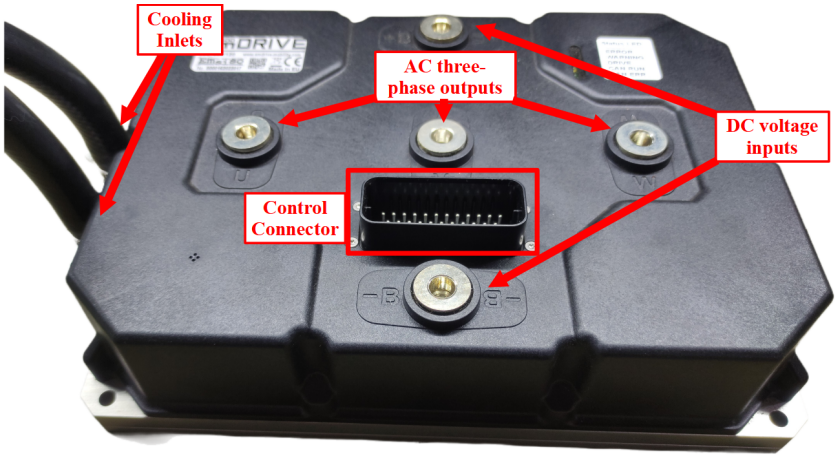

Figure 11. emDrive 500 inverter.

The inverter has a nominal power of 62 kW, input voltage between 30 and 120 V, nominal current of 500 A, and switching frequency of 16 kHz. It is built using discrete MOSFETs and has current measurements in two phases, in addition to MOSFET temperature monitoring, as shown in Figure 12. The switch control is internal, making it possible for the user to modify the controller gains and send the torque or speed setpoints.

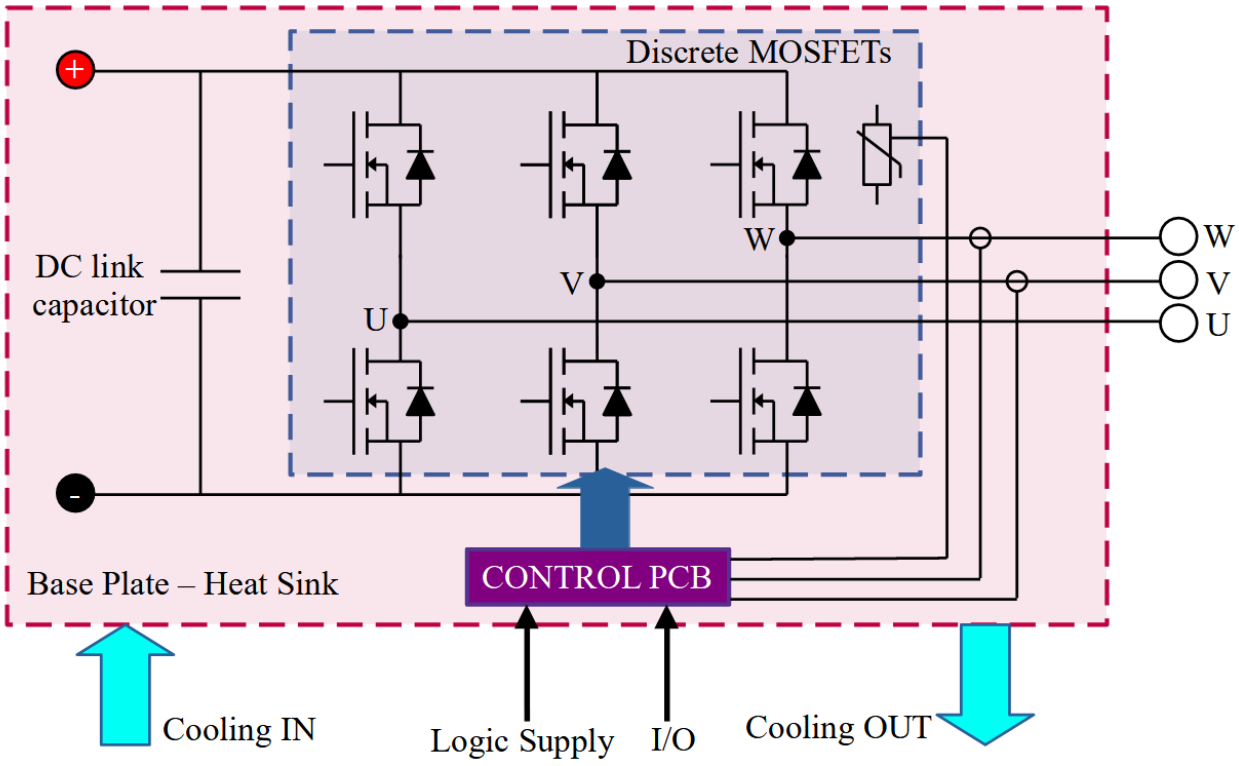

Figure 12. emDrive 500 inverter diagram.

5.3. Power Cables

The high-voltage cables used in vehicle applications have special characteristics and specific standards. According to UN/ECE 100, high voltage is defined as vehicle electrical systems supplied with voltages above 60 V_{dc} [17]. According to the ISO 6722-1 standard [20], high-voltage cables in electric vehicles must be predominantly orange in color and must have a shielding mesh to reduce electromagnetic interference problems in the vehicle circuits.

The cross-section of the power cables should be as small as possible, as this facilitates installation in reduced spaces such as vehicles. In the case of heavy vehicles that will not have their chassis structure changed, this becomes fundamental.

To reduce the cross-section of the cables, cables with insulating material that withstand high temperatures must be used. In this case, cables with silicone insulation are the most recommended, as they can work with temperatures up to 180 °C [48]. For comparative purposes, cables used in residential and industrial electrical installations typically have polyvinyl chloride (PVC), high-density crosslinked polyethylene (XLPE), or ethylene propylene rubber (EPR) insulation and typically operate at temperatures up to 90 °C [49].

Considering the maximum average power shown in Table 2 and the minimum battery voltage shown in Table 3, the calculated current for this case is 277 A. A shielded cable with a copper core and silicone insulation was defined, with an operating temperature of up to 180 °C with a section of 50 mm^2 to meet the current demands.

5.4. DC/DC Converters

An important component of the electric drive is the dc/dc converter. Depending on how the hybridization topology is planned, there will be a dc/dc converter between the battery bank and the inverters. The specification of this converter must cover the input and output voltage of the converter and the maximum operating power of the system. It is worth noting that this dc/dc converter must be bidirectional for recharging batteries in a hybrid system and recovering energy from braking.

The other dc/dc converter present in the application is the auxiliary power module (APM). The purpose of the APM is to convert the high voltage of the batteries into a lower voltage (e.g., 12 to 14 V) for powering non-propulsion loads, such as the controllers and the cooling system. The specification of this converter must also cover the input and output voltage of the converter and the maximum operating power of the system, taking into account loads not related to propulsion. Taking into account such power parameters and that it works with a range of 72 V to 96 V, the APM specified for the application is the Elcon TDC-IY-108-12 [50].

6. Design of Switching and Protection Components

6.1. High Voltage Interlock Loop (HVIL)

A high-voltage interlock loop circuit (HVIL) is a safety feature of electric and hybrid vehicles that protects users during vehicle assembly, repair, maintenance, and operation. It routes through each vehicle's high-voltage connector, checking for any disconnected cables, either intentionally or due to breakage, de-energizing the vehicle [51]. Figure 13 shows an example of an HVIL circuit.

Vehicle electrical connectors have low-voltage terminals for connecting the HVIL circuit, as shown in Figure 14. When connecting the cables, the contact is closed, causing the circuit to be closed. In case of disconnection, this contact is opened and the detector is activated, opening a power relay connected to the battery, for example.

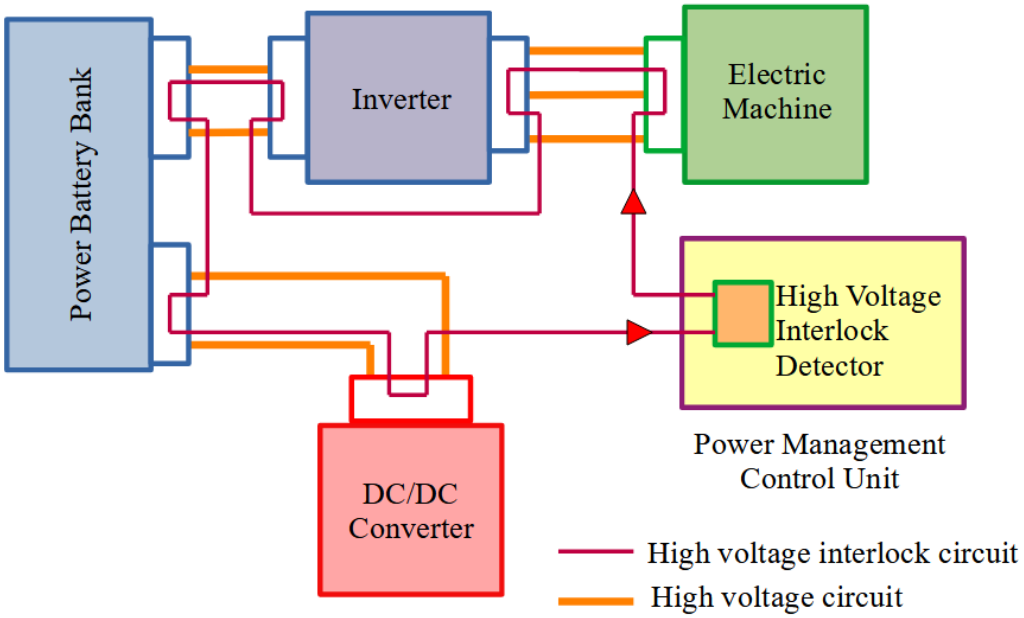

Figure 13. High Voltage Interlock Loop (HVIL).

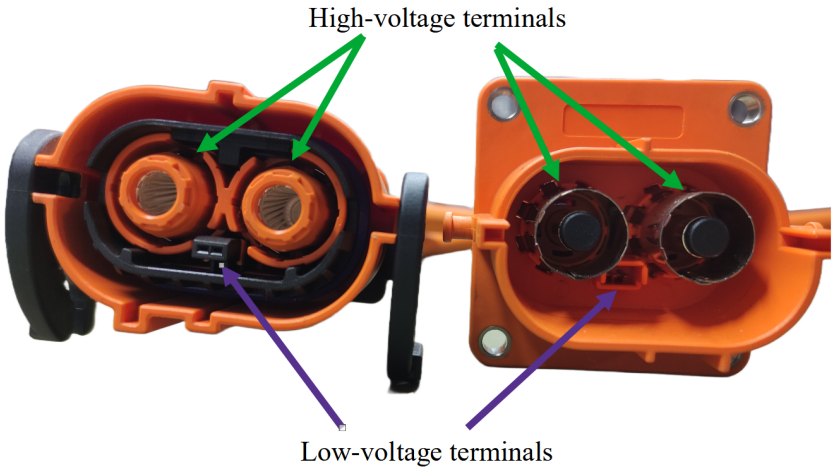

Figure 14. Power connectors with low-voltage terminals.

6.2. Insulation Monitoring Device (IMD)

The Insulating Monitoring Device (IMD) is a device that measures the insulation between the high-voltage terminals of the battery and the ground of the vehicle; that is, its chassis. It is a safety component that guarantees that there are no accidents with electric shock for vehicle users in case of contact with the housing. One of the main standards governing insulation monitoring devices is IEC 61557-8 [52].

To specify the IMD, it is necessary to check the operation voltage and the communication resources in case of insulation failure. Some devices have programmable alerts to indicate low insulation levels and more critical situations.

6.3. Pre-Charge Circuit

Arc extinction in direct current is more difficult due to the absence of cyclical crossing of the current through zero, which is the most relevant characteristic for vehicle relays and fuses. Thus, fuses intended for vehicle use must meet standards such as ISO 8820 [53] and they should meet quality standards such as ISO/TS 16949 [54], an ISO technical specification that governs standards for automotive quality systems existing in the world, such as

Brazilian, American, German, French and Italian standards within the global automotive industry. This quality standard is also desired for relays used in vehicle applications.

Figure 15 shows a diagram of the connection of the batteries to the inverter. Some protection components for the drive system items are necessary to maintain their integrity in case of possible failures in the operation. Among them, the main ones are relays, fuses, and pre-charge resistors.

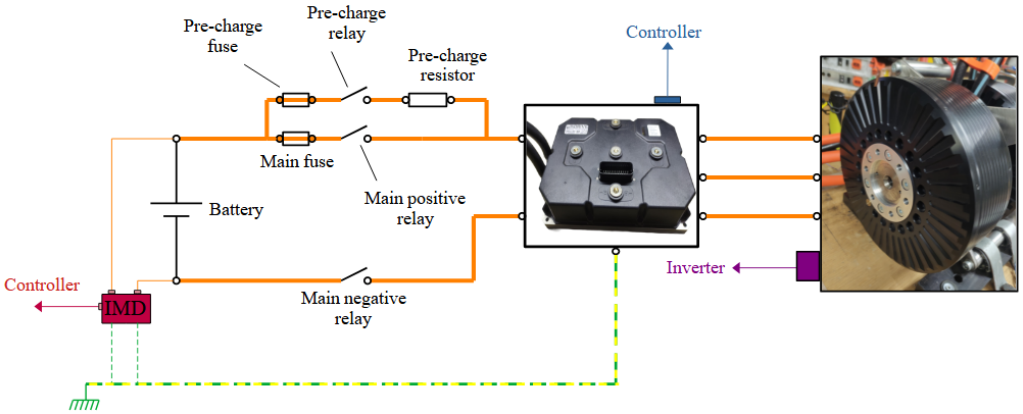

Figure 15. Diagram of the connection of the batteries to the inverter.

The pre-charge circuit aims to charge the dc bus capacitors more smoothly, avoiding a high initial current that could damage the dc link capacitors. The pre-charge circuit consists of a contactor, a fuse, and a resistor. By connecting the batteries through the pre-charge circuit, the capacitor will charge exponentially with the RC time constant.

In some cases, the inverter datasheet informs the characteristics of the components of the pre-charge and main circuits. If this is not available, the preload resistor must be specified according to the following criteria [55]:

- Maximum voltage;
- Maximum energy;
- Power overload capacity of the resistors during the pre-charge period (energy dissipation capacity).

The maximum resistor voltage is the voltage on the dc link. The maximum energy is the energy stored in the capacitor at the end of pre-charge. The power dissipation capacity is the initial maximum power dissipation of the resistor ($P = V_{dc}^2/R$). The fuse and pre-charge relay must take into account the maximum current during pre-charge, which is given by the ratio of dc link voltage to resistance. For the emDrive 500 inverter, a 8 A fuse [56] was specified.

The pre-charge relay was specified with a breaking capacity of 30 A at 450 Vdc [57]. The inverter manufacturer recommends a pre-charge resistor with 27 Ω and 534 W peak [46]. High pulse capacity wire resistors are recommended, such as the HS series manufactured by Tyco [58].

6.4. Main Protection Circuit

The power relay and main fuse must be specified with minimum voltage above maximum dc link voltage and current above the overload current. As with the pre-charge circuit, the inverter manual usually has this information. Fuses must be fast-acting and suitable for vehicle application, meeting the ISO 8820 standard.

The emDrive 500 manual recommends a fast-acting fuse to be installed between the battery bank and the inverter that has a maximum current of 630 A and a minimum voltage of 150 V_{dc}. Considering the battery bank data (Table 3), it can be seen that:

- For analysis of the charging process, the battery bank admits a current of 444.4 A (max. 10 min.) or 277.8 A (continuous) in the condition of minimum voltage of the pack (72 V) that matches with the worst case in terms of current values.
- For the discharge process, the battery bank is capable of much higher current values in short time intervals. As the fuse is a fast-acting one, care must be taken to ensure that improper actuation does not occur within these limits.

However, as the average drive power was specified at 20 kW and with a minimum voltage totaling 72 V, the value of the charge current drops to 277 A and the maximum discharge current will not exceed 500 A. For reducing costs, a 300 A fuse was chosen, which allows the load condition to overload for 10 min, does not act in the discharge condition of 500 A and protects the battery in a discharged condition of 1000 A for 10 s [59]. Figure 16 shows the current versus time curve for fuse actuation, with emphasis on the aforementioned discharge conditions.

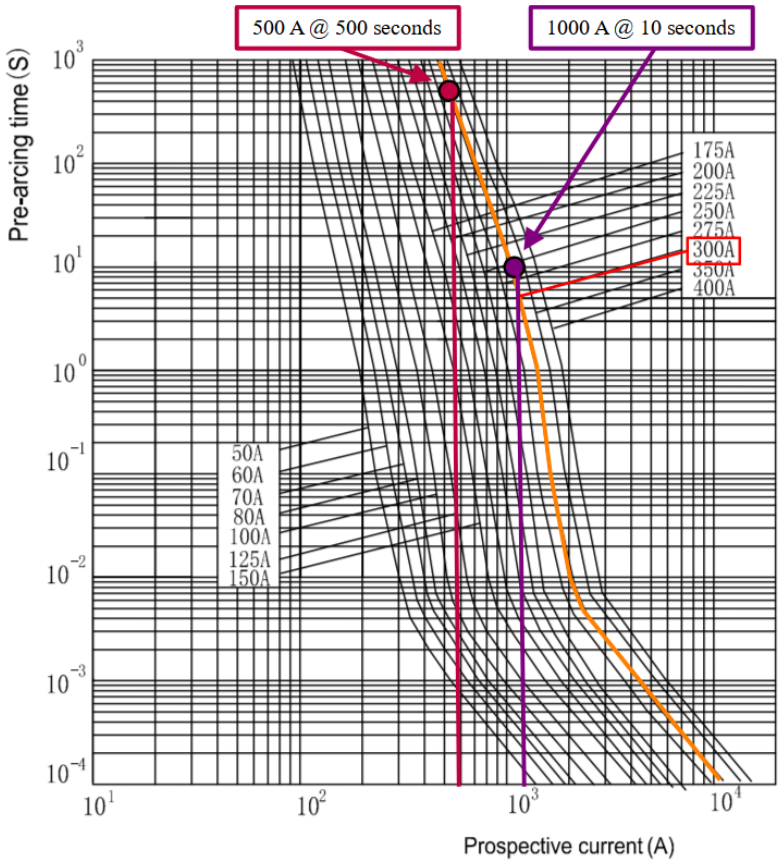

Figure 16. Curve current *vs* time of 300 A fuse.

The main relay was specified to meet the continuous and transient needs of the project, with a continuous conduction current of 500 A, in addition to the ability to interrupt 2 kA operating with voltages up to 320 V_{cc} [60].

7. Key Points for Electric Drive System Design

The key points for specifying the components of the electric drive system of an HCM can be summarized in the following points:

I. Define the hybridization strategy by observing cost and degrees of freedom.
II. Check the power of the operation performed by the HCM.
III. Define the size of the battery bank according to the desired maximum volume.
    - Define the BMS that meets the specifications of the battery bank.

IV. Define electrical machines, inverters, and dc/dc converters based on operating power and battery bank voltage.
- Check whether the electrical machine delivers the power and torque required for operation at the desired operating speed.
- Check whether the inverters and dc/dc converters have the desired communication protocol.

V. Define high voltage cables in compliance with current regulations.
- To reduce the cross-section of the cables, use insulation material that withstands higher temperatures.

VI. Define protection and switching elements.
- Establish the proper HVIL and IMD to protect users and service technicians.
- Correctly specify the pre-charge resistors according to the maximum voltage, maximum energy, and power overload capacity.
- Check if the main fuse operates both in nominal operation and in motor overloads, without it tripping in advance.

8. Test Bench

Figure 17 shows the 3D design of the backhoe electric drive system test bench. The workbench has two electrical machines coupled so that one of them can emulate the behavior of the ICE or the hydraulic pump coupled with the backhoe implements.

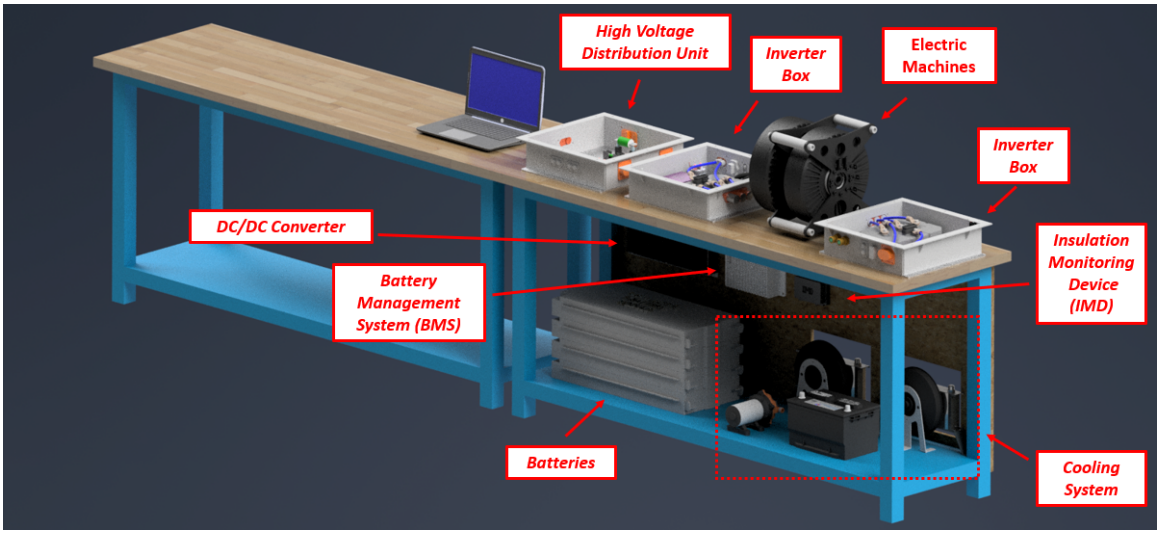

Figure 17. 3D design of the backhoe electric drive system test bench.

The high-voltage distribution unit (HVDU) and inverter boxes were built to accommodate the power components for installation on the backhoe loader. Figure 18 shows the built HVDU that will accommodate the switching and protection components and will distribute the voltage from the batteries to the inverters and the dc/dc converter. As the boxes and power cables are being installed on the backhoe loader, a provisional prototype bench was built for testing and can be seen in Figure 19.

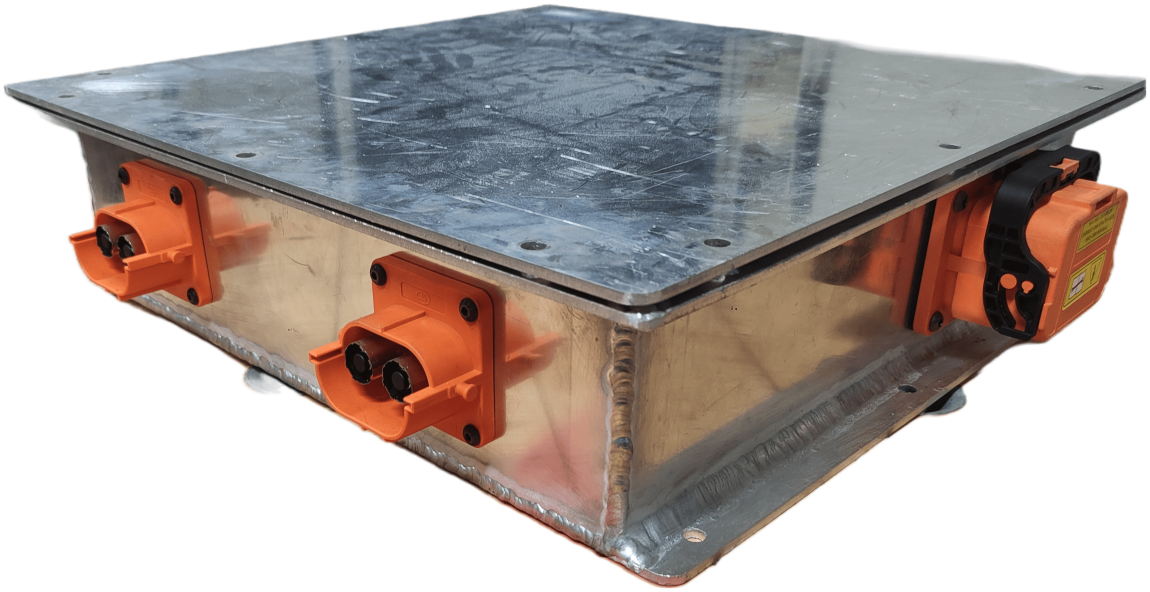

Figure 18. High Voltage Distribution Unit (HVDU).

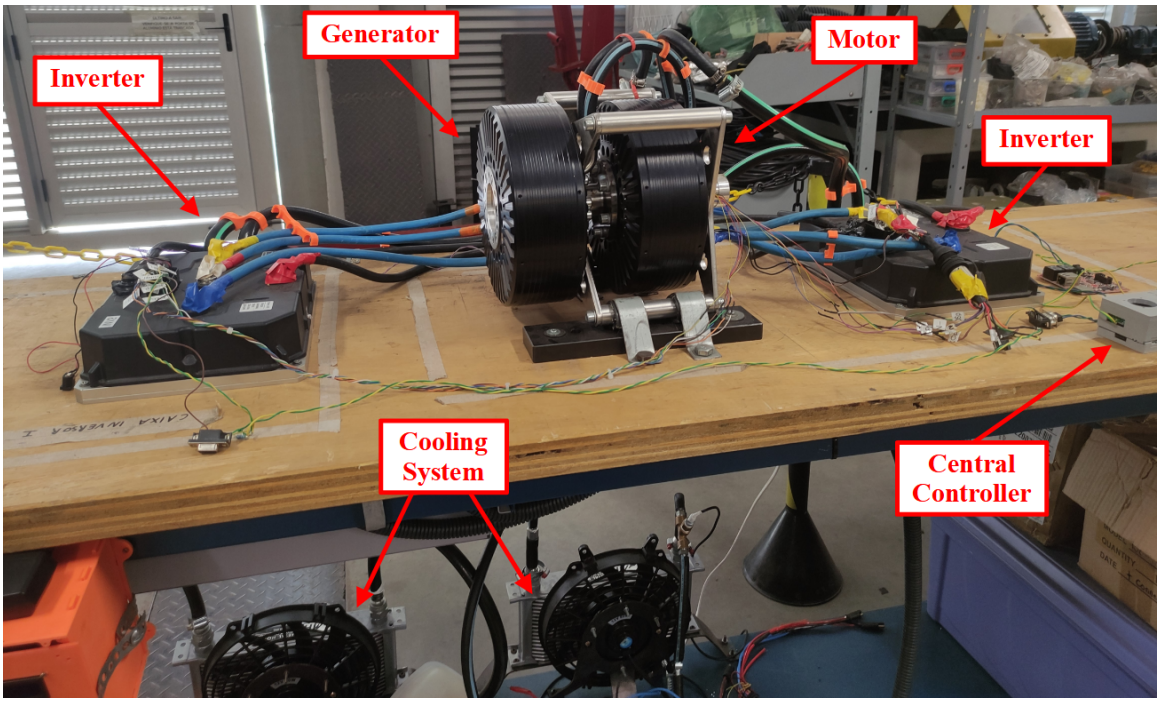

Figure 19. Prototype test bench.

9. PMSM Drive Modeling, Control and Simulation

The motor drive control provided by the inverter manufacturer [46] can be represented by the block diagram of Figure 20. It can be split in four main parts: plant model, current (torque) control, Maximum Torque Per Ampere (MTPA) strategy, speed control and Field Weakening Control (FWC).

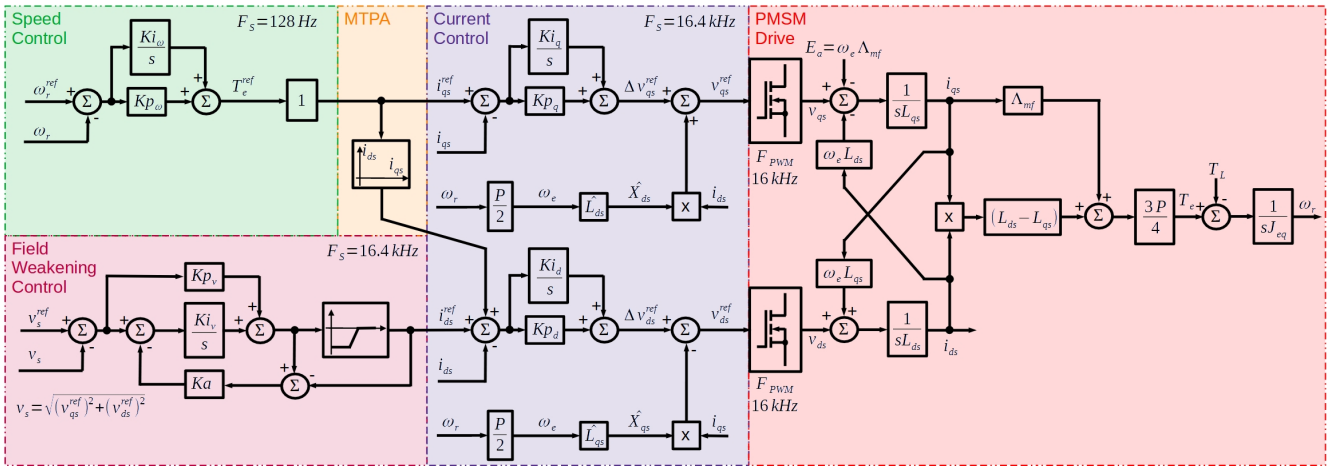

Figure 20. PMSM Drive Control.

9.1. Plant Model Description

The Permanent Magnet Synchronous Machine (PMSM) was modeled in a rotating reference frame (d and q axes) synchronous with the rotor flux angle, as usually applied in vector control of ac drives [61]. This model can be described by Equations (1)–(5).

$$v_{ds} = r_s i_{ds} + \frac{d\lambda_{ds}}{dt} - \omega_e \lambda_{qs} \tag{1}$$

$$v_{qs} = r_s i_{qs} + \frac{d\lambda_{qs}}{dt} + \omega_e \lambda_{ds} \tag{2}$$

$$\lambda_{ds} = L_{ds} i_{ds} + \Lambda_{mf} \tag{3}$$

$$\lambda_{qs} = L_{qs} i_{qs} \tag{4}$$

$$T_e = \frac{3}{2}\frac{P}{2}\left(\lambda_{ds} i_{qs} - \lambda_{qs} i_{ds}\right) \tag{5}$$

where the decomposed voltage components at the inverter output (v_{ds} and v_{qs}) are subtracted (q axis only) from the PMSM internal voltage (E_a) and applied to the axis inductances (L_{ds} and L_{qs}), resulting in the current components (i_{ds} and i_{qs}). The PMSM internal voltage is proportional to the electrical frequency (ω_e) and to the magnets flux (Λ_{mf}). There are also induced voltages from one axis to the other that are proportional to the speed, inductances and currents.

Replacing (3) and (4) in (5), the torque equations can be presented in the alternative forms of (6) and (7). The former clearly shows how i_{ds} can impact the net flux of the PMSM and how the q-axis components can counterbalance the effects of an $i_{ds} \neq 0$. The last one evidences the field and reluctance torque components.

$$T_e = \frac{3}{2}\frac{P}{2}\left[(\Lambda_{mf} + L_{ds} i_{ds}) i_{qs} - L_{qs} i_{qs} i_{ds}\right] \tag{6}$$

$$T_e = \frac{3}{2}\frac{P}{2}\left[\Lambda_{mf} i_{qs} + (L_{ds} - L_{qs}) i_{ds} i_{qs}\right] \tag{7}$$

The electromagnetic torque (T_e) is the result of two components: a predominant one from the product $\frac{3P}{4}\Lambda_{mf} i_{qs}$ (where P is the number of magnetic poles) and a minor one, called reluctance torque, from the product $\frac{3P}{4}(L_{ds} - L_{qs}) i_{ds} i_{qs}$. The reluctance torque component is present when using PMSMs with inner-mounted magnets, where $L_{ds} \neq L_{qs}$.

For PMSMs with surface-mounted magnets, $L_{ds} \approx L_{qs}$, therefore there is no appreciable reluctance torque component.

Finally, the mechanical system is modeled considering the dynamic relation presented in (8) [62].

$$T_e = J_{eq}\frac{d\omega_r}{dt} + b\omega_r + T_L \tag{8}$$

where J_{eq} is the total effective inertia of the load and motor as seen by the motor, b is the viscous friction coefficient, ω_r is the mechanical angular speed and T_L is the load torque. In Figure 20, the viscous friction action was neglected (i.e., $b = 0$).

9.2. Control Description

The current control is then implemented with a proportional–integral feedback controller for each axis current. The outputs of these controllers, augmented with proper terms to decouple the voltage actions between axes, are the voltages references used for the generation of the pulse pattern by the semiconductors. Ki_q, Kp_q, Ki_d and Kp_q are, respectively, the q-axis and d-axis integral and proportional gains. The superscript ^{ref} indicates a reference signal and the hat over a symbol indicates an estimated parameter.

A speed control is used upstream to the q-axis current controller to produce the torque (current) reference. It has integral and proportional gains named Ki_ω and Kp_ω, respectively. Some constructive constants should be included between the cascaded controllers in order to promote a proper conversion from Nm to A, but they are absent. Notably, when using the PMSM as a generator instead of a motor, the speed control is either eliminated (torque control mode of operation) or substituted by another upstream control (e.g., dc bus voltage control).

The d-axis reference can be set to zero, resulting in the Field Oriented Control (FOC) [61], or an MTPA strategy can be used to take advantage of the reluctance torque feature of inner magnets mounted PMSM [63]. In this inverter, the MTPA strategy is simply a second-order polynomial function with coefficients free to be adjusted by the user [46]. The input to this function is the q-axis current.

In high speeds, the internal voltage E_a can be greater than the maximum allowed by the inverter dc voltage level. This can also happen in situations in which the battery system is directly connected to the inverter dc bus and the battery State-of-Charger (SoC) is low. In both situations, there is a need for a Field Weakening Control (FWC) strategy that makes use of a value of i_{ds} that properly reduces the net flux in the PMSM and, therefore, the voltage [64].

In the inverter used in this application, the FWC strategy is composed of a feedback controller for the stator voltage (v_s). This stator voltage controller is applied upstream to the d-axis current controller. The output of this controller has a saturation that automatically makes $i_{ds} = 0$ when the output tends to be greater than zero (which would result in a field strengthening action). This implementation is based in typical FWC implementations applied to dc motors [65]. Here, there is the drawback that the feedback is not directly measured, but calculated from the outputs of the current controllers instead.

Due to the use of saturation in the output of the voltage controller, a proper anti-windup system is required to avoid the undesired accumulation of error by the integral term of the controller. The anti-windup implemented in this inverter is based on the classical approach of subtracting from the integrator input, the difference of the unsaturated and saturated values, multiplied by an anti-windup gain (Ka) [66].

9.3. Controllers Adjust

In order to adjust the rotating reference frame current controllers, the disturbance to output relationships, defined as dynamic stiffness in motion control [67], was applied. For the current controllers, this relationship is described by (9).

$$\left|\frac{E_a}{i_{dq}}\right| = sL_{dqs} + Kp_{dq} + \frac{Ki_{dq}}{s} \tag{9}$$

For the speed controller, the dynamic stiffness is defined by (10), where J_{eq} is the total inertia of the mechanical system (i.e., motor and load inertia) and T_L is the load torque. This equation considers that this control loop is much slower (e.g., a decade) than the downstream one.

$$\left|\frac{T_L}{\omega_r}\right| = sJ_{eq} + Kp_{\omega} + \frac{Ki_{\omega}}{s} \tag{10}$$

When the FWC is active (i.e., its output is not saturated), the dynamic stiffness of the stator voltage control loop in cascade with the d-axis current control loop is given by (11). This function was defined, assuming that $v_{qs}^2 >> v_{ds}^2$, and consequently $v_s \approx v_{qs}$.

$$\frac{\Lambda_{mf}}{v_s} = \frac{\frac{s^2}{\omega_e} + s\left(Kp_v \cdot Kp_d + \frac{Kp_d}{\omega_e \cdot L_{ds}}\right) + \left(Kp_v \cdot Ki_d + Ki_v \cdot Kp_d + \frac{Ki_d}{\omega_e \cdot L_{ds}}\right) + \frac{Ki_v \cdot Ki_d}{s}}{s^2 + s\frac{Kp_d}{L_{ds}} + \frac{Ki_d}{L_{ds}}} \tag{11}$$

The denominator is entirely defined by the previously presented d-axis current controllers parameters. The numerator has three poles that can be approximately defined as – if sufficiently spaced among themselves—(12), (13) and (14), from the fastest to the slowest one. All of them are affected by the gains of the stator voltage controller (Ki_v and Kp_v).

$$\omega_1 = Kp_d\left(\omega_e Kp_v + \frac{1}{L_{ds}}\right) \tag{12}$$

$$\omega_2 = \frac{Kp_v Ki_d + Kp_d Ki_v + \frac{Ki_d}{\omega_e L_{ds}}}{Kp_v Kp_d + \frac{Kp_d}{\omega_e L_{ds}}} \tag{13}$$

$$\omega_3 = \frac{Ki_v Ki_d}{Kp_v Ki_d + Kp_d Ki_v + \frac{Ki_d}{\omega_e L_{ds}}} \tag{14}$$

The controllers design (see Table 4) of this work can be summarized as follows:

- The current controller gains were chosen to locate the poles of (9) spaced a decade apart, with the fastest one being ten times slower than the switching frequency (F_{PWM}) of 16 kHz, which is also the sampling frequency (F_S) of this part of the control;
- The speed controller gains were chosen to have a dynamic stiffness (10) with fastest pole ten times slower than the sampling frequency (128 Hz, in this case) and to be spaced a decade apart;
- MTPA is not applied, since the motor is of the axial flux type with almost no reluctance torque ($L_{ds} \approx L_{qs}$);
- The FWC gains were designed to maintain the d-axis current control loop speed (i.e., $Kp_v = 0$), to keep the poles of (13) and (14) in frequencies 5 and 20 times less than (12). The anti-windup gain was chosen to be simultaneously high enough to avoid the integration of error during the saturation and sufficiently limited to allow a fast transition from the saturated to the unsaturated mode.

Table 4. Controllers Design in SI base units.

Parameter	Value	Parameter	Value
L_{ds}	10.3 µH	L_{qs}	10.6 µH
J_{eq}	0.0766 kg · m^2	Ka	0.29 Ω [1]
Kp_{dq}	0.0733 Ω	Ki_{dq}	50.6 Ω/s
Kp_{ω}	6.2 Nm · s/rad	Ki_{ω}	49.5 Nm/rad
Kp_{v}	0 Ω^{-1}	Ki_{v}	291 kΩ^{-1}/s

[1] Adjusted considering a base speed of 2200 rpm.

One of the challenges when using commercial inverters is that they seldom use SI units in their software. In the case of the applied system, the units are as follows:

- For the current, they use a unit called *quants* that is constant. The only exception is the output of the FWC, which uses Ampere;
- For the voltage, they use a unit also called *quants*. However, it is not the same unit from the current and, furthermore, it is proportional to the measured dc voltage;
- For the speed, the controller uses rpm instead of rad/s.

Table 5 presents gains in the inverter's system of units, which is the value that is actually entered in the controller.

Table 5. Controllers Design in the inverter's system of units.

Parameter	Value	Parameter	Value
$C2Q$ [1]	$(2^{15}-1)\times 10^{-3}$	$V2Q$ [2]	1.457×10^{3}
$N2\omega$ [3]	$\pi/30$ rad/ (s·rpm)	Ka	424 quants/A
Kp_{dq}	3.257 quants/quants	Ki_{dq}	2250 quants/(quants·s)
Kp_{ω}	0.645 Nm/rpm	Ki_{ω}	5.2 Nm / (rpm·s)
Kp_{v}	0 A/quants	Ki_{v}	200 A/(quants·s)

[1] Current to *quants* (of current) conversion factor; [2] Voltage to *quants* (of voltage) conversion factor considering 65 V in the dc bus; [3] Conversion factor from Nm·s/rad to Nm/rpm.

9.4. Simulation Results

The system described in this work was simulated in the time domain using the Simulink environment from MATLAB [68]. The power plant was simulated using the following blocks from Simscape Electrical Specialized Power Systems Library [69]:

- Permanent Magnet Synchronous Machine Block: This block implements the model described by Equations (1)–(5) for the electromagnetic system and (8) for the mechanical one. Its inputs are the three-phase voltages and the mechanical torque.
- Two-Level Converter Block: This block implements a three-phase, two level converter according to the one resented in Figure 11. Its inputs are the switches gating signals and it has five electrical ports: two for the dc link and three for the ac terminals.
- Series RLC Branch Block: It implements the differential equations of a series connected circuit composed by a resistor, a capacitor, and an inductor. It is used to model the capacitive dc link (refer to Figure 11).
- DC Voltage Source Block: It implements an ideal dc voltage source. This is used to model the voltage source used in the experimental set-up (see Section 10).

The control system was modeled by using math operations, discrete, user-defined functions and other blocks from the basic Simulink library.

The PMSM input torque curve used for this simulation is the one represented in Figure 21, which is the one used in the experimental results of Section 10. An efficiency of

92% was considered to take into account the absence of a generator attached to the motor in the simulation.

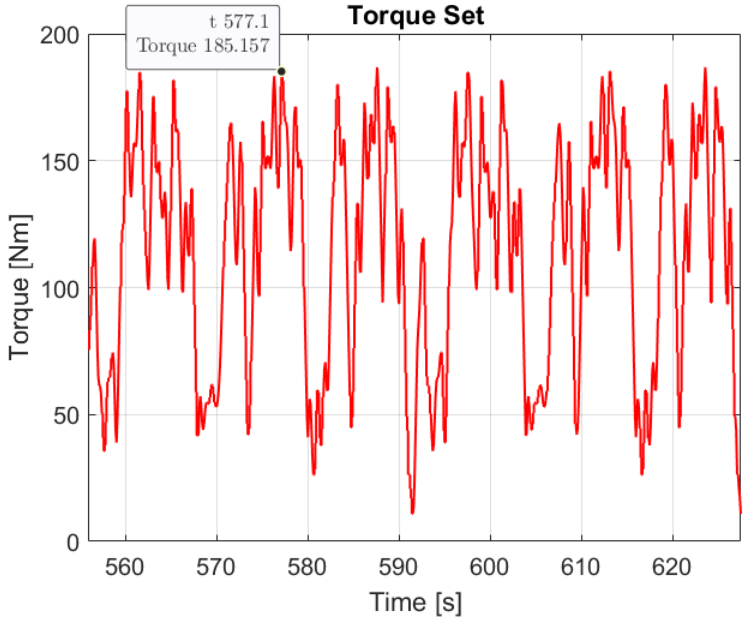

Figure 21. Target torque applied to the generator.

Figure 22 shows the simulation results for speed, electromagnetic torque and power at the PMSM motor. A maximum ripple in steady state of 430 rpm can be observed for the rotor speed, which corresponds to approximately 24% of the reference speed.

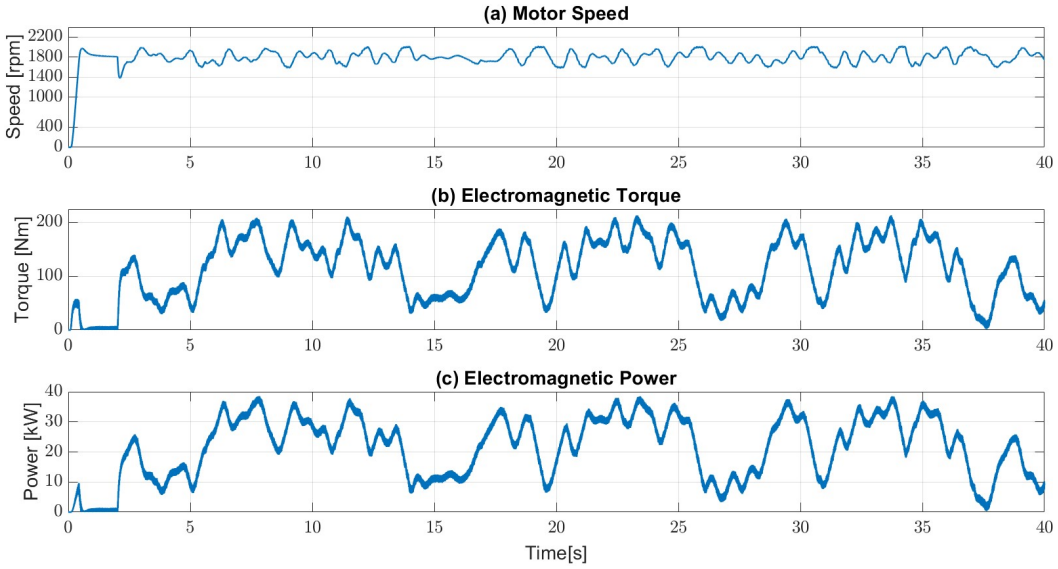

Figure 22. PMSM variables: (**a**) rotor speed; (**b**) electromagnetic torque; (**c**) electromagnetic power.

Figure 23 shows the three-phase currents of the PMSM stator during the simulation. Although the continuous motor drive current limit (450 A_{rms}) was surpassed several times, the transitory limit (800 A_{rms} for 1 min) was not.

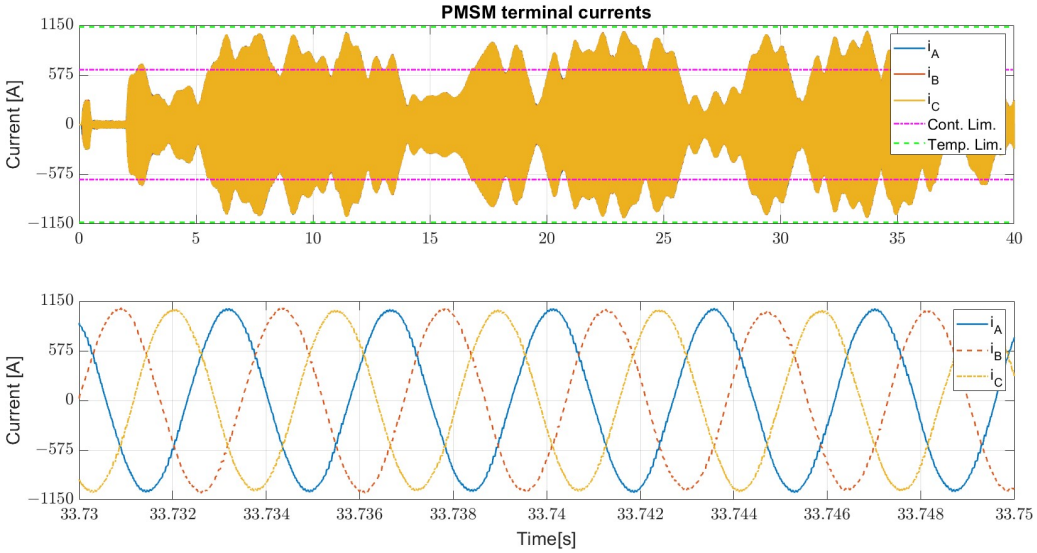

Figure 23. PMSM Currents.

Figure 24 shows the dq-axes currents and references voltages at the PMSM stator during the simulation. It shows that field weakening operation was not necessary, since $i_d = 0$ all the time (i.e., operation in FOC).

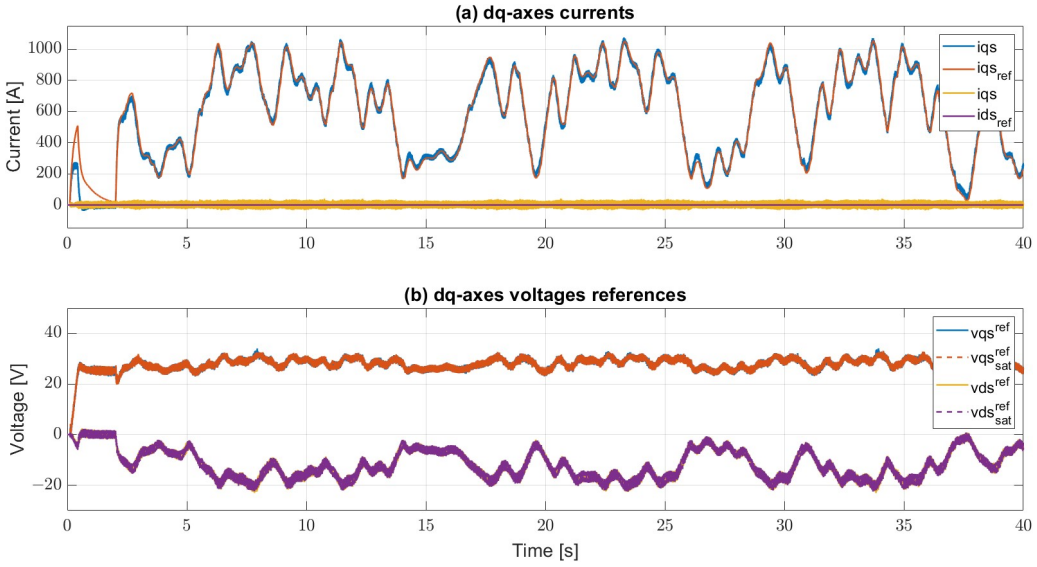

Figure 24. dq axes variables: (**a**) currents; (**b**) voltages.

Finally, to test the FWC, the dc voltage was reduced to 50 V and a ramp was applied from 1000 rpm to 1800 rpm, as presented in Figure 25. This shows that the d-axis current increased automatically when the internal generated voltage was close enough to the inverter output voltage limit. This test was performed at no load.

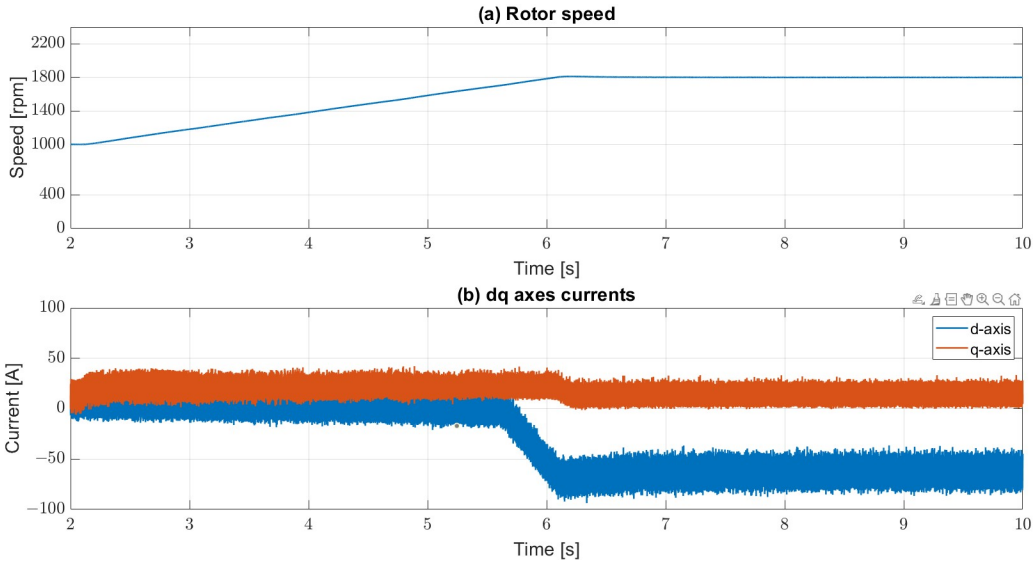

Figure 25. Field Weakening Control Simulation: (**a**) rotor speed; (**b**) dq axes currents.

10. Experimental Results

To evaluate some of the functionalities of the electric drive system, the bench was submitted to a back-to-back test, whose scheme can be seen in Figure 26. With this, it is possible to simultaneously analyze the machine operating as a motor and as a generator for integration in the backhoe loader's electric drive system.

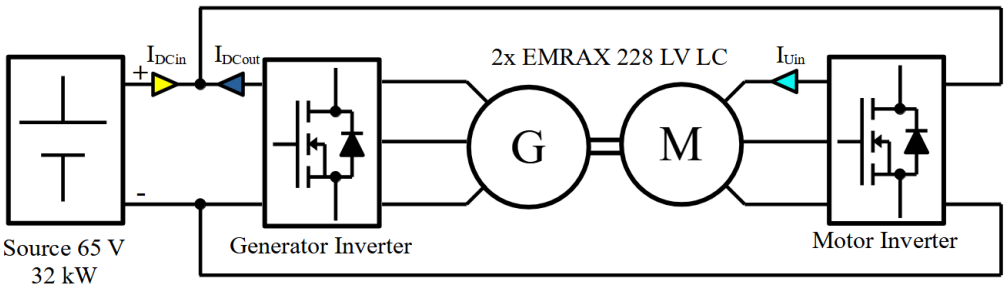

Figure 26. Back-to-back test scheme.

A Regatron TC.GSS.32.65 voltage source provides the system composed of inverters and machines, supplying only losses and reducing energy consumption. The reference speed of the electric motor was 1800 rpm. Figure 21 shows the target torque curve applied to the generator based on the power shown in Figure 6.

Figure 27 shows the velocity of the machines. There is a maximum speed overshoot of 408 rpm, equivalent to 22.6% of the rated speed. There is also a maximum undershoot of 393 rpm, about 21.6% of the nominal system speed.

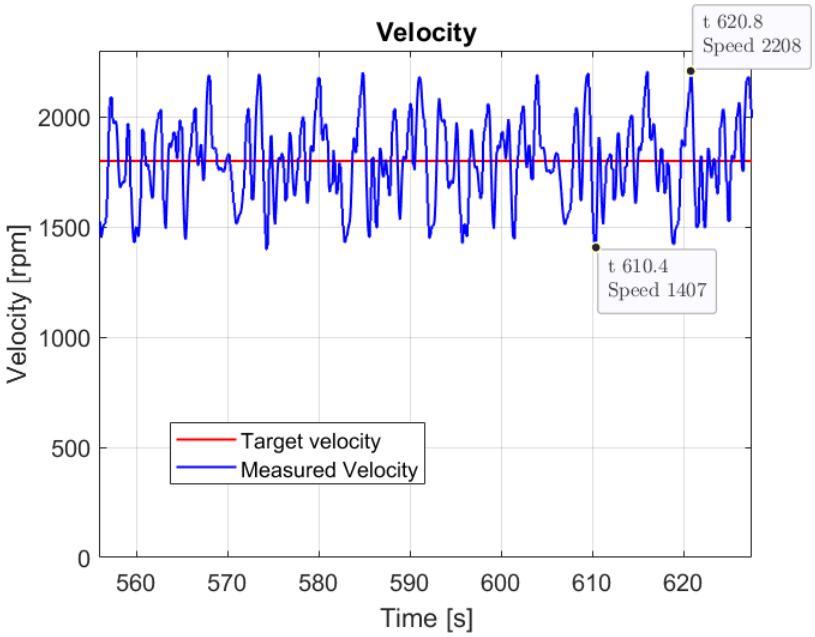

Figure 27. Target velocity and measured velocity.

Finally, in order to verify the proper functioning of the test bench in field weakening conditions, the dc voltage was intentionally reduced to 50 V and a ramp from 1000 rpm to 1800 rpm was commanded, as presented in Figure 28. The results shows that the speed was tracked by using a negative value of d-axis current when the calculated stator voltage surpassed the reference one (Figure 29). This test was performed in no load conditions.

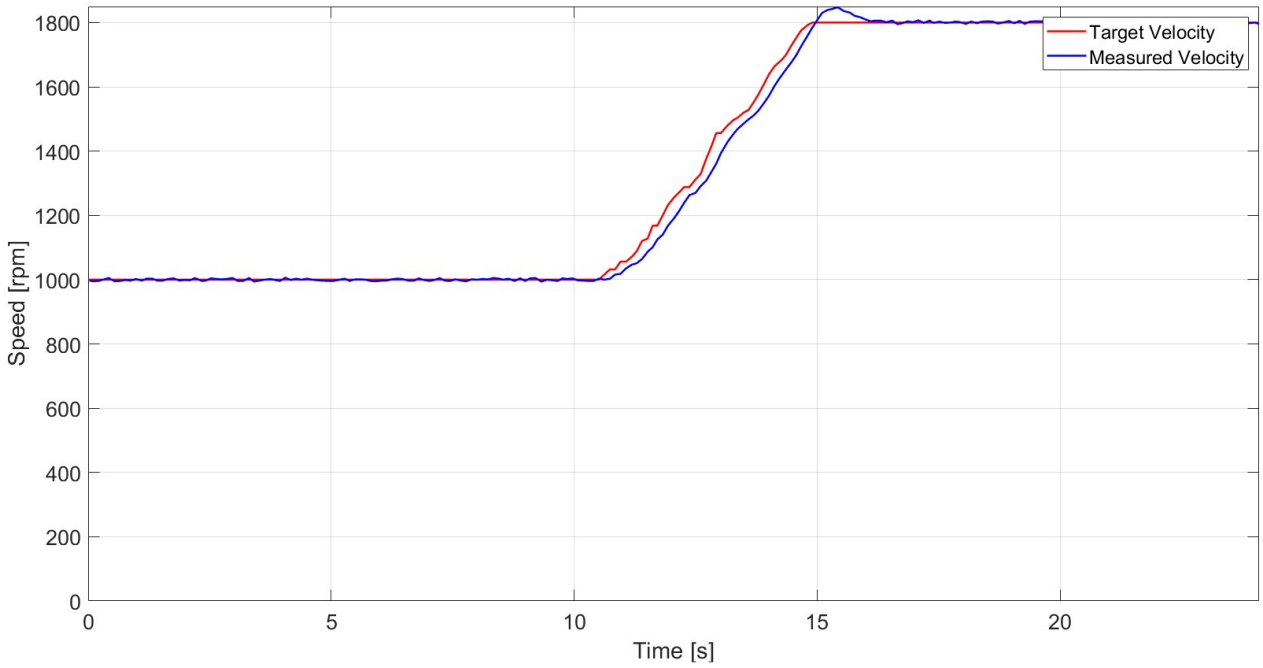

Figure 28. Speed command and measurement for the field weakening operation test.

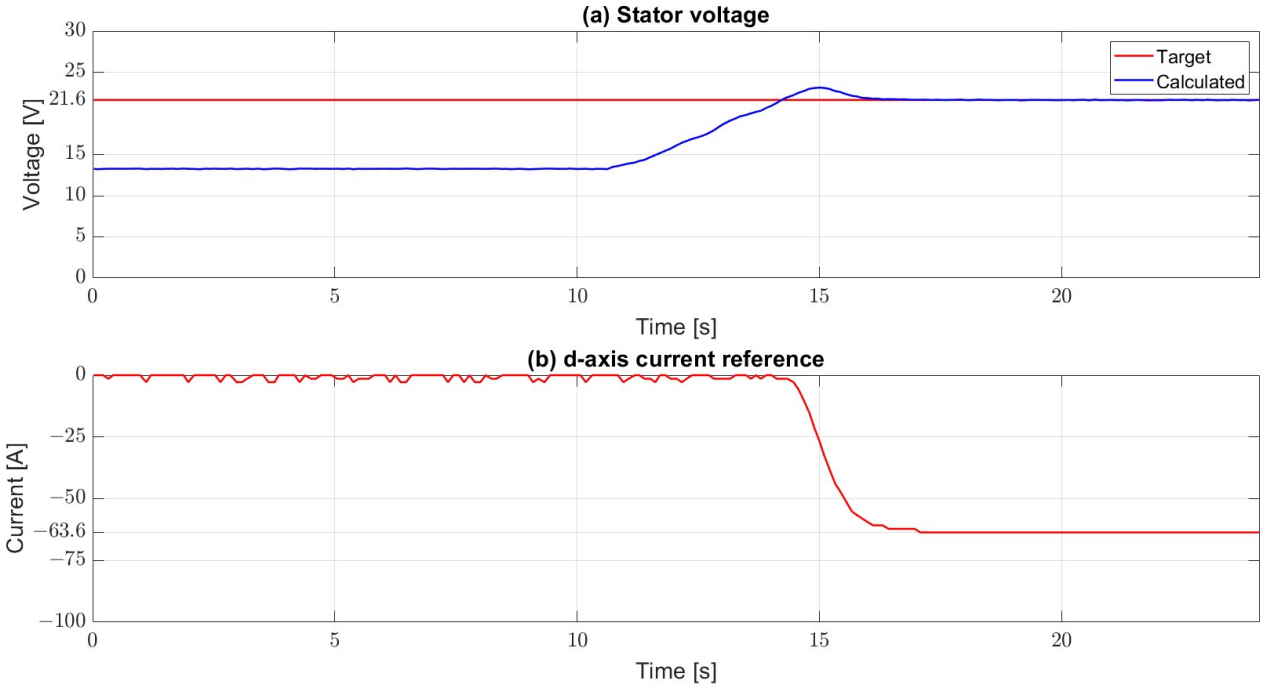

Figure 29. (**a**) Stator voltage and (**b**) d-axis current reference for the field weakening operation test.

11. Discussions

The simulation and experimental results for the speed control, Figures 22 and 27, respectively, present a poor speed regulation with a large ripple during operation. These results are a combined function of the choice for the system operation point and the restrictions imposed by the control implemented in the inverter. Here, some suggestions for improvement are presented and analyzed. Although they could, theoretically, be employed all at once, the results are presented individually to give an understanding of the actual impact provided by each one.

First of all, the speed controller has a sample rate of only 128 Hz, which limits its bandwidth to a decade below this frequency. In order to test a faster speed compensator, both the sample frequency and the gains were multiplied by ten. Figure 30a shows the results, with no significant ripple in the rotor speed. For the system under analysis, this could be implemented only with an external speed controller sending the torque (q-axis current) reference for the inverter working in the torque control mode.

Some improvements in the implemented control are also analyzed, including an estimation of the internal generated voltage at the q-axis current controller output and the inclusion of the appropriate PMSM constants between the output of the speed compensator and the input of the q-axis current one. Figure 31 shows a modified version of the control diagram with these suggestions.

Figure 30b presents the speed regulation result. Currently, the rotor speed ripple is less than 7% (approximately 120 rpm). The modification on the q-axis current control needs to be performed in the inverter firmware, but the addition of the torque to current conversion factor could be performed either in the inverter or in an external speed controller. The right conversion from Nm to A has greater impact on the performance than the E_a estimation, since the q-axis current controller is already fast enough.

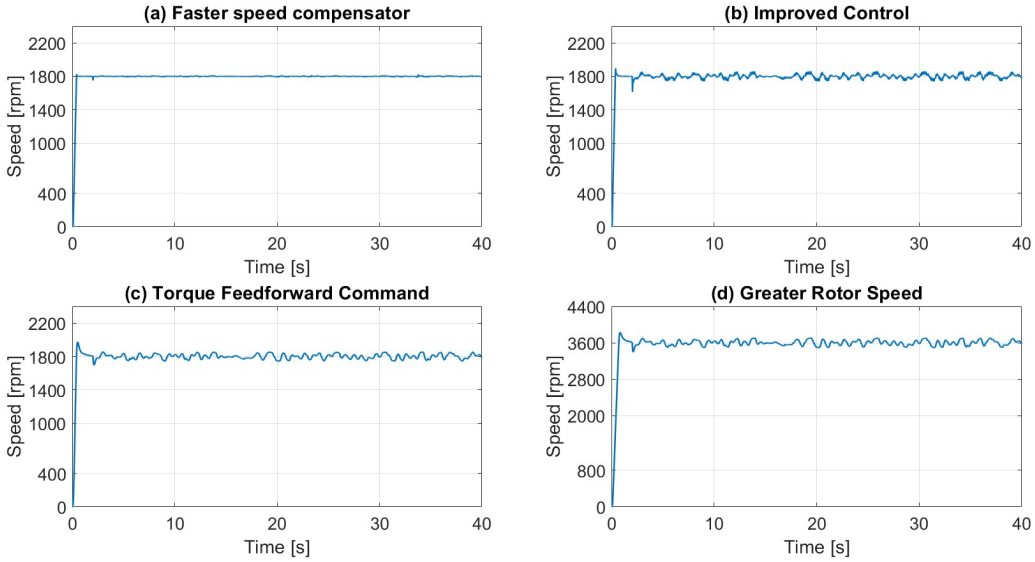

Figure 30. Speed Simulation Results with proposed modifications: (**a**) faster speed compensator; (**b**) control improvements; (**c**) torque feedforward; (**d**) greater rotor speed.

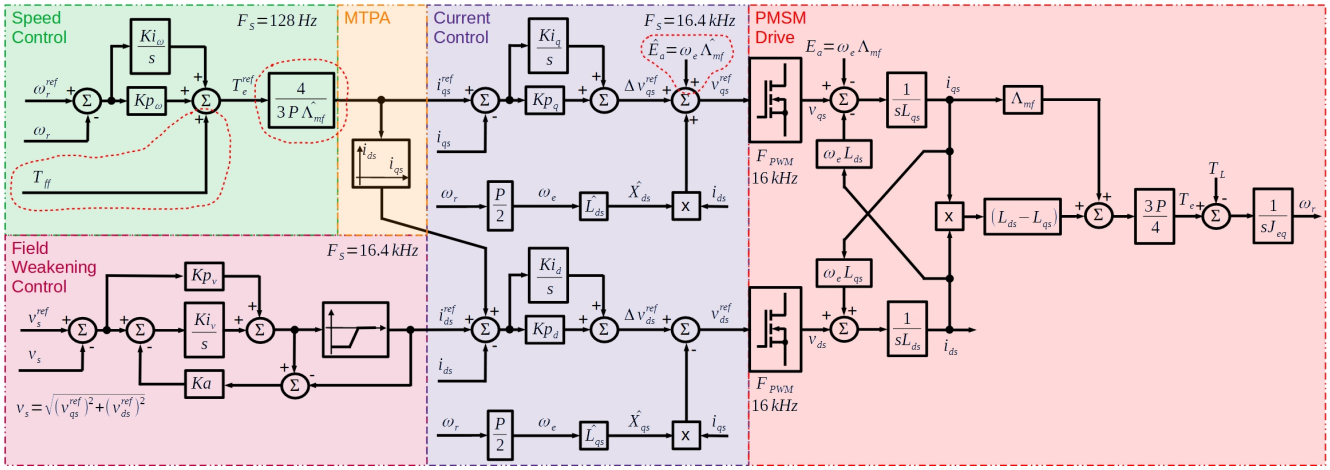

Figure 31. PMSM Drive Control with proposed improvements.

Figure 31 shows another possible modification: the insertion of a torque feedforward command (T_{ff}). This feedforward would not be subjected to the low dynamic of the speed compensator, granting it the job of correcting only the errors in the estimated parameters and in the T_{ff} itself.

Figure 30c shows the result for a T_{ff} 20% lower than the actual one. This error was intentionally included to verify the impact of inaccuracies in the feedforward. Even so, a ripple of only about 6.2% (110 rpm) was present in the simulated system. The implementation of a torque feedforward in the motor would require transducers to measure the hydraulic pump output power (fluid flow × pressure), which can be expensive.

Finally, a solution with no impact on the control system at all is the increase in the operation speed. Figure 30d shows the result for twice the original speed with the same load power. The torque ripple of about 200 rpm represents less than 5.7% of the new reference speed. This result is achieved because the inertial kinetic energy is proportional to the square of the speed, resulting in four times more mechanical energy being stored in the system to aid absorption of the load torque variations.

This new point of operation would require a gearbox to couple the PMSM with the hydraulic pump and, at the same time, an increase in the dc bus voltage in order to be successfully implemented.

The correct design of the electric drive system and its control is essential for the effectiveness of the energy management strategy. By validating the electrical operation of the backhoe implements, it is necessary to implement the energy management strategy, which aims to change the ICE's operating regions to reduce fuel consumption. The proof of consumption reduction with the implementation of the proposed energy management strategy will be the object of work in the real prototype, which is under construction.

12. Conclusions

This work presents the main characteristics for the development of a good project of the electric drive system aiming at the electrification of a heavy vehicle, taking into account the limitations imposed for volume reduction and minimization of the alteration of the initial characteristics of the machine. In addition to the technical details of the component specification, it is necessary to pay attention to current regulations and safety aspects.

Another aspect evaluated in this paper is the control of the electric drive. The computational simulation of the operation of the system with the load profile of the heavy off-road vehicle implements allows the identification of problems and the evaluation of alternative solutions, such as: increasing the controllers bandwidth, the system speed, including feedforward command and improving the control implementation by using a model-based approach. The alternatives can contribute to the expected operation of the backhoe to achieve the objectives of reducing fuel consumption.

A proper electrical drive design is essential for the implementation of energy management strategies aimed at reducing fuel consumption and will define the necessary parameters for the design of cooling and communication systems. It is equally important to properly tune the controllers to obtain a satisfactory performance from the motor drive system.

Author Contributions: Conceptualization, D.A.d.L.B., M.d.F.R., T.M.P. and T.P.C.; methodology, D.A.d.L.B. and T.M.P.; software, D.A.d.L.B., T.M.P. and T.P.C.; validation, D.A.d.L.B., M.d.F.R., T.M.P. and T.P.C.; formal analysis, D.A.d.L.B. and T.M.P.; investigation, D.A.d.L.B., M.d.F.R. and T.M.P.; resources, I.A.P., T.A.C.M., A.N. and B.d.J.C.F.; data curation, D.B and T.M.P.; writing—original draft preparation, D.B and T.M.P.; writing—review and editing, D.A.d.L.B. and T.M.P.; visualization, D.A.d.L.B. and T.M.P.; supervision, I.A.P., T.A.C.M., A.N. and B.d.J.C.F.; project administration, I.A.P., T.A.C.M., A.N. and B.d.J.C.F.; funding acquisition, I.A.P., T.A.C.M., A.N. and B.d.J.C.F. All authors have read and agreed to the published version of the manuscript.

Funding: This research was funded by Fundação de Desenvolvimento da Pesquisa (FUNDEP)—Rota 2030/Linha V, grant number 27192.03.01/2020.15-00.

Institutional Review Board Statement: Not applicable.

Informed Consent Statement: Not applicable.

Data Availability Statement: Not applicable.

Acknowledgments: This work was also supported by the Coordenação de Aperfeiçoamento de Pessoal de Nível Superior (CAPES), by the Conselho Nacional de Desenvolvimento Científico e Tecnológico (CNPq) and by the Fundação de Amparo à Pesquisa do Estado de Minas Gerais (FAPEMIG).

Conflicts of Interest: The authors declare no conflict of interest.

Abbreviations

The following abbreviations are used in this manuscript:

APM	Auxiliary Power Module.
BMS	Battery Management System.
CAN	Controller Area Network.
DC	Direct Current.
EPR	Ethylene Propylene Rubber.
FOC	Field Oriented Control.
FWC	Field Weakening Control.
HCM	Hybrid Construction Machinery.
HVDU	High Voltage Distribution Unit.
HVIL	High Voltage Interlock Loop.
ICE	Internal Combustion Engine.
IMD	Insulation Monitoring Device.
LC	Liquid Cooled.
LV	Low Voltage.
MTPA	Maximum Torque Per Ampere.
PMSM	Permanent Magnet Synchronous Machine.
PVC	Polyvinyl Chloride.
SoC	State of Charge.
XLPE	High-density crosslinked polyethylene.

References

1. Davis, S.C.; Boundy, R.G. Transportation Energy Databook: Edition 40. 2022. Available online: https://tedb.ornl.gov/wp-content/uploads/2022/03/TEDB_Ed_40.pdf (accessed on 25 January 2023).
2. Liu, Y.; Li, Z.; Chen, Y.; Zhao, K. A Novel Fuel-Cell Electric Articulated Vehicle and Its Drop-and-Pull Transport System. *Energies* **2020**, *13*, 3632. [CrossRef]
3. Mendes, F.E.G.; Brandao, D.I.; Maia, T.; de Filho, J.C.B. Off-Road Vehicle Hybridization Methodology Applied to a Tractor Backhoe Loader. In Proceedings of the IEEE Transportation Electrification Conference and Expo (ITEC), Detroit, MI, USA, 19–21 June 2019; pp. 1–6. [CrossRef]
4. Somà, A. Trends and Hybridization Factor for Heavy-Duty Working Vehicles. In Hybrid Electric Vehicles; InTech: London, UK, 2017; pp. 3–32. (accessed on 27 January 2023) [CrossRef]
5. Masrur, M.A. Hybrid and Electric Vehicle (HEV/EV) Technologies for Off-Road Applications. *Proc. IEEE* **2021**, *109*, 1077–1093. [CrossRef]
6. Munoz, L.E.; Blanco, J.C.; Barreto, J.P.; Rincon, N.A.; Roa, S.D. Conceptual design of a hybrid electric off-road vehicle. In Proceedings of the 2012 IEEE International Electric Vehicle Conference, Greenville, SC, USA, 4–8 March 2012; pp. 1–8. [CrossRef]
7. Rossi, C.; Pontara, D.; Falcomer, C.; Bertoldi, M.; Mandrioli, R. A Hybrid–Electric Driveline for Agricultural Tractors Based on an e-CVT Power-Split Transmission. *Energies* **2021**, *14*, 6912. [CrossRef]
8. Gao, Y.; Ehsani, M. Parametric design of the traction motor and energy storage for series hybrid off-road and military vehicles. *IEEE Trans. Power Electron.* **2006**, *21*, 749–755. [CrossRef]
9. Troncon, D.; Alberti, L.; Bolognani, S.; Bettella, F.; Gatto, A. Electrification of agricultural machinery: A feasibility evaluation. In Proceedings of the 2019 Fourteenth International Conference on Ecological Vehicles and Renewable Energies (EVER), Monte-Carlo, Monaco, 8–10 May 2019; pp. 1–7. [CrossRef]
10. Dalboni, M.; Santarelli, P.; Patroncini, P.; Soldati, A.; Concari, C.; Lusignani, D. Electrification of a Compact Agricultural Tractor: A Successful Case Study. In Proceedings of the 2019 IEEE Transportation Electrification Conference and Expo (ITEC), Detroit, MI, USA, 19–21 June 2019; pp. 1–6. [CrossRef]
11. Troncon, D.; Alberti, L. Case of Study of the Electrification of a Tractor: Electric Motor Performance Requirements and Design. *Energies* **2020**, *13*, 2197. [CrossRef]
12. Ge, L.; Quan, L.; Zhang, X.; Zhao, B.; Yang, J. Efficiency improvement and evaluation of electric hydraulic excavator with speed and displacement variable pump. *Energy Convers. Manag.* **2017**, *150*, 62–71. [CrossRef]
13. Liao, Y.G.; O'Malley, M.; Quail, A. Experimental evaluation of parallel hybrid medium-duty tactical truck. In Proceedings of the 2012 IEEE Transportation Electrification Conference and Expo (ITEC), Dearborn, MI, USA, 18–20 June 2012; pp. 1–6. [CrossRef]
14. Zhao, D.; Stobart, R.; Dong, G.; Winward, E. Real-time energy management for diesel heavy duty hybrid electric vehicles. *IEEE Trans. Control Syst. Technol.* **2015**, *23*, 829–841. [CrossRef]
15. Park, J.; Murphey, Y.L.; Masrur, M.A. Intelligent Energy Management and Optimization in a Hybridized All-Terrain Vehicle With Simple On–Off Control of the Internal Combustion Engine. *IEEE Trans. Veh. Technol.* **2016**, *65*, 4584–4596. [CrossRef]

16. Zhang, W.; Wang, J.; Du, S.; Ma, H.; Zhao, W.; Li, H. Energy Management Strategies for Hybrid Construction Machinery: Evolution, Classification, Comparison and Future Trends. *Energies* **2019**, *12*, 2024. [CrossRef]
17. Regulation No. 100 Rev.3-Uniform Provisions Concerning the Approval of Vehicles with Regard to Specific Requirements for the Electric Power Train. Available online: https://unece.org/transport/documents/2022/03/standards/regulation-no-100-rev3 (accessed on 26 January 2023).
18. *ISO 6469-2*; Electrically Propelled Road Vehicles—Safety specifications—Part 2: Vehicle Operational Safety. Available online: https://www.iso.org/standard/81346.html (accessed on 26 January 2023).
19. *ISO 6469-3:2021*; Electrically Propelled Road Vehicles—Safety Specifications—Part 3: Electrical Safety. Available online: https://www.iso.org/standard/81746.html (accessed on 26 January 2023).
20. *ISO 6722-1:2011*; Road Vehicles—60 V and 600 V Single-Core Cables—Part 1: Dimensions, Test Methods and Requirements for Copper Conductor Cables. Available online: https://www.iso.org/standard/50022.html (accessed on 26 January 2023).
21. *ISO 17409:2020*; Electrically Propelled Road Vehicles—Conductive Power Transfer—Safety Requirements. Available online: https://www.iso.org/standard/72880.html (accessed on 26 January 2023).
22. *ISO 15118-1:2019*; Road Vehicles—Vehicle to Grid Communication Interface—Part 1: General Information and Use-Case Definition. Available online: https://www.iso.org/standard/69113.html (accessed on 26 January 2023).
23. *ISO 26262-1:2018*; Road Vehicles—Functional Safety—Part 1: Vocabulary. Available online: https://www.iso.org/standard/68383.html (accessed on 26 January 2023).
24. *BS EN 60529:1992+A2:2013*; Degrees of Protection Provided by Enclosures (IP Code). Available online: https://www.en-standard.eu/bs-en-60529-1992-a2-2013-degrees-of-protection-provided-by-enclosures-ip-code (accessed on 26 January 2023).
25. *BS EN IEC 61851-1:2019*; Electric Vehicle Conductive Charging System General Requirement. Available online: https://www.en-standard.eu/bs-en-iec-61851-1-2019-electric-vehicle-conductive-charging-system-general-requirements (accessed on 26 January 2023).
26. *IEC 62485-3:2014*; Safety Requirements for Secondary Batteries and Battery Installations—Part 3: Traction Batteries. Available online: https://webstore.iec.ch/publication/7092 (accessed on 26 January 2023).
27. *SAE J2344*; Guidelines for Electric Vehicle Safety. Available online: https://www.sae.org/standards/content/j2344_202010/ (accessed on 26 January 2023).
28. *SAE J1797*; Recommended Practice for Packaging of Electric Vehicle Battery Modules (STABILIZED Aug 2016). Available online: https://www.sae.org/standards/content/j1797_201608/ (accessed on 26 January 2023).
29. *SAE J1939*; Serial Control and Communications Heavy Duty Vehicle Network—Top Level Document. Available online: https://www.sae.org/standards/content/j1939_201808/ (accessed on 26 January 2023).
30. Palavicino, P.C.; Sarlioglu, B.; Bobba, D.; Lee, W.; Minav, T. Eletrification of Hydraulic Systems using High Efficiency Permanent Magnet Motors. In Proceedings of the 12th International Fluid Power Conference (12th IFK), Dresden, Germany, 12–14 October 2020.
31. Un-Noor, F.; Scora, G.; Wu, G.; Boriboonsomsin, K.; Perugu, H.; Collier, S.; Yoon, S. Operational Feasibility Assessment of Battery Electric Construction Equipment Based on In-Use Activity Data. *Transp. Res. Rec.* **2021**, *2675*, 809–820. [CrossRef]
32. Kagoshima, M.; Sora, T.; Komiyama, M. Power Source Device for Working Machine, U.S. Patent 7525206B2, 28 April 2009.
33. Wang, J.; Yang, Z.; Liu, S.; Zhang, Q.; Han, Y. A comprehensive overview of hybrid construction machinery. *Adv. Mech. Eng.*. **2016**, *8*, 1–15. [CrossRef]
34. Immonen, P. Energy Efficiency of a Diesel-Electric Mobile Working Machine. Ph.D. Thesis, Lappeenranta University of Technology, Lappeenranta, Finland, 2013. Available online: https://lutpub.lut.fi/bitstream/handle/10024/90573/isbn9789522654151.pdf?isAllowed=y&sequence=2 (accessed on 27 February 2023).
35. Ratzinger, J.M.; Buchberger, S.; Eichlseder, H. Electrified powertrains for wheel-driven non-road mobile machinery.*Automot. Engine Technol.* **2021**, *6*, 1–13. [CrossRef]
36. Jalil, N.; Kheir, N.A.; Salman, M. A rule-based energy management strategy for a series hybrid vehicle. In Proceedings of the 1997 American Control Conference (Cat. No.97CH36041), Albuquerque, NM, USA, 6 June 1997; Volume 1, pp. 689–693. [CrossRef]
37. Wang, H.; Wang, Q.; Hu, B. A review of developments in energy storage systems for hybrid excavators. *Autom. Constr.* **2017**, *80*, 1–10. [CrossRef]
38. Dong, J.; Huang, Y.; Jin, L.; Lin, H. Comparative Study of Surface-Mounted and Interior Permanent-Magnet Motors for High-Speed Applications. *IEEE Trans. Appl. Supercond.* **2016**, *26*, 1–4. [CrossRef]
39. He, T.; Zhu, Z.; Eastham, F.; Wang, Y.; Bin, W.; Wu, D.; Gong, L.; Chen, J. Permanent Magnet Machines for High-Speed Applications. *World Electr. Veh. J.* **2022**, *13*, 18. [CrossRef]
40. Sitapati, K.; Krishnan, R. Performance comparisons of radial and axial field, permanent-magnet, brushless machines. *IEEE Trans. Ind. Appl.* **2001**, *37*, 1219–1226. [CrossRef]
41. Huang, R.; Song, Z.; Zhao, H.; Liu, C. Overview of Axial-Flux Machines and Modeling Methods. *IEEE Trans. Transp. Electrif.* **2022**, *8*, 2118–2132. [CrossRef]
42. Hayes, J.; Goodarzi, G. *Electric Powertrain: Energy Systems, Power Electronics and Drives for Hybrid, Electric and Fuel Cell Vehicles*; John Wiley & Sons: Hoboken, NJ, USA, 2018.
43. Aghabali, I.; Bauman, J.; Kollmeyer, P.J.; Wang, Y.; Bilgin, B.; Emadi, A. 800-V Electric Vehicle Powertrains: Review and Analysis of Benefits, Challenges, and Future Trends. *IEEE Trans. Transp. Electrif.* **2021**, *7*, 927–948. [CrossRef]

44. EMRAX Innovative E-Motors EMRAX 228. Available online: http://emrax.com/e-motors/emrax-228/ (accessed on 27 January 2023).
45. Reimers, J.; Dorn-Gomba, L.; Mak, C.; Emadi, A. Automotive Traction Inverters: Current Status and Future Trends. *IEEE Trans. Veh. Technol.* **2019**, *68*, 3337–3350. [CrossRef]
46. Emsiso emDrive 500. Available online: https://www.emdrive-mobility.com/portfolio/emdrive-500/ (accessed on 29 January 2023).
47. CANopen—The Standardized Embedded Network. Available online: https://www.can-cia.org/canopen/ (accessed on 29 January 2023).
48. Coroflex—High-Voltage and Charging Cables. Available online: https://www.coroflex-cable.com/en/high-voltage-cables (accessed on 27 January 2023).
49. Power Cable Product Families. Available online: https://www.belden.com/products/cable/power-cable (accessed on 26 January 2023).
50. DC/DC Converter 1000W Isolated 74-162 Volts. Available online: https://www.evwest.com/catalog/product_info.php?cPath=33&products_id=546&osCsid=19d45f613fc078cf0276c4ab8e9e7940 (accessed on 1 February 2023).
51. TESLA Tech Note: HVIL Diagnostic Guide. Available online: https://static.nhtsa.gov/odi/tsbs/2014/SB-10052449-4313.pdf (accessed on 28 January 2023).
52. *IEC 61557-8:2014*; Electrical Safety in Low Voltage Distribution Systems up to 1000 V a.c. and 1500 V d.c.-Equipment for Testing, Measuring or Monitoring of Protective Measures—Part 8: Insulation Monitoring Devices for IT Systems. International Electrotechnical Commission (IEC): Geneva, Switzerland, 2014.
53. *ISO ISO 8820-8:2012*; Road vehicles—Fuse-links—Part 8: Fuse-Links with Bolt-in Contacts (Type H and J) with Rated Voltage of 450 V. International Organization for Standardization: Geneva, Switzerland, 2012.
54. *ISO/TS 16949:2009*; Quality Management Systems—Particular Requirements for the Application of ISO 9001:2008 for Automotive Production and Relevant Service Part Organizations. Available online: https://www.iso.org/standard/52844.html (accessed on 28 January 2023).
55. Regenerative Frequency Converter CFW-11—User's Manual. Available online: https://static.weg.net/medias/downloadcenter/h65/h1e/WEG-10005022198-14064791-r00-CFW11RB-users-manual-en.pdf (accessed on 30 January 2023).
56. Adler Electric AE3 EV Fuse. Available online: https://www.adlerelectric.com/products/detail/151 (accessed on 30 January 2023).
57. Littelfuse DCNSEV30-B-DCNSEV30 Series. Available online: https://www.littelfuse.com/products/dc-solenoids-and-relays/high-voltage-dc-contactor-relays/dcnsev30/dcnsev30-b.aspx (accessed on 31 January 2023).
58. TE Connectivity HSA5027RJ Datasheet. Available online: https://www.te.com/usa-en/product-3-1625984-9.html (accessed on 31 January 2023).
59. Bussmann Series High Speed Fuses-FWH-300A. Available online: https://www.eaton.com/us/en-us/skuPage.FWH-300A.specifications.html (accessed on 31 January 2023).
60. TE Connectivity-EV200AAANA. Available online: https://www.te.com/usa-en/product-1618002-7.html (accessed on 31 January 2023).
61. Novotny, D.W.; Lipo, T.A. *Vector Control and Dynamics of AC Drives*; Oxford University Press: New York, NY, USA, 1996; p. 440.
62. Slemon, G.R. Dynamic Relations for Drive Systems. In *Electric Machines and Drives*; Addison-Wesley Publishing Company: Reading, PA, USA, 1992; pp. 354–360.
63. Yuniarto, M.N.; Sidharta, I.; Yohanes, Y.; Nugraha, Y.U. On the Development and Experimental Validation of a Novel and Intuitive Interior Permanent Magnet Synchronous Motor Controller for Electric Vehicle Application. *World Electr. Veh. J.* **2022**, *13*, 107. [CrossRef]
64. Parreiras, T.M.; Brandão, D.A.L.; Maia, T.A.C.; Pires, I.A.; Nascimento, A.; Cardoso, B.J. Field Weakening Strategies to Suppress Intermediate DC-DC Conversion Stages in Hybrid Construction Machinery. In Proceedings of the 2022 IEEE Transportation Electrification Conference and Expo, Asia-Pacific (ITEC Asia-Pacific), Haining, China, 28–31 October 2022.
65. Leonhard, W. Control of a Separately Excited DC Machine. In *Control of Electrical Drives*, 3rd ed.; Springer: Berlin, Germany, 2001; pp. 77–96.
66. Franklin, G.F.; Powell, J.D.; Emani-Naeini, A. Basic Properties of Feedback. In *Feedback Control of Dynamic Systems*, 4th ed.; Prentice Hall: Upper Saddle River, NJ, USA, 2002; pp. 200–269.
67. Lorenz, R.D.; Lipo, T.A.; Novotny, D.W. Motion control with induction motors. *Proc. IEEE* **1994**, *82*, 1215–1240. [CrossRef]
68. The MathWorks, Inc. Simulink-Simulation and Model-Based Design. Available online: https://www.mathworks.com/products/simulink.html (accessed on 24 March 2023).
69. The MathWorks, Inc. Specialized Power Systems: Model Electrical Power Systems Using Specialized Components and Algorithms. Available online: https://www.mathworks.com/help/sps/specialized-power-systems.html (accessed on 24 March 2023).